T2R2 東京科学大学 リサーチリポジトリ
Science Tokyo Research Repository

論文 / 著書情報
Article / Book Information

題目(和文)	
Title(English)	Directional Normalized Energy Stability Margin and Non-Tumbling Gait for Robust Legged Locomotion
著者(和文)	LAZARENKOEVGENY
Author(English)	Evgeny Lazarenko
出典(和文)	学位:博士(工学), 学位授与機関:東京工業大学, 報告番号:甲第9291号, 授与年月日:2013年9月25日, 学位の種別:課程博士, 審査員:福島 E 文彦,大熊 政明,小田 光茂,松永 三郎,塚越 秀行,野田 篤司,廣瀬 茂男
Citation(English)	Degree:Doctor (Engineering), Conferring organization: Tokyo Institute of Technology, Report number:甲第9291号, Conferred date:2013/9/25, Degree Type:Course doctor, Examiner:,,,,,,
学位種別(和文)	博士論文
Type(English)	Doctoral Thesis

Powered by T2R2 (Science Tokyo Research Repository)

Directional Normalized Energy Stability Margin and Non-Tumbling Gait for Robust Legged Locomotion

Evgeny Lazarenko

A dissertation submitted to the

Department of Mechanical and Aerospace Engineering

in partial fulfillment of the requirments for the degree of

Doctor of Engineering

Graduate School of Engineering

Tokyo Institute of Technology
Tokyo, JAPAN

September 2013

©Tokyo Institute of Technology 2013. All rights reserved.

Doubt grows with knowledge.

Acknowledgments

First and foremost, I would like to thank professor Shigeo Hirose for being my advisor for three years, from April 2010 to April 2013. I am infinitely grateful for his invaluable support and insights. Professor Hirose is not just a distinguished researcher and scholar, but a man of amazing human qualities. He is the best advisor I have ever had.

I want to express gratitude to professor Edwardo F. Fukushima who is my current advisor. He has always been a patient and attentive guide, and his advice helped me to navigate through the last semester of my doctoral course, which is arguably one of the most critical period in every student's life.

I would also like to thank professor Gen Endo for his comments and quirky insights about this research. Undoubtedly, he helped me to look at this work from many different angles.

Also, I would like to thank all of the students of Fukushima Laboratory for bearing with my character for more than three years, and especially Satoshi Kitano, who also works in the field of walking robots and has given me a lot of valuable comments about my research.

Last but not least, I want to thank you, a person who is now reading this work. I made my best to make this thesis easy to understand by explaining all the concepts thoroughly, in clear and simple language. I appreciate your taking time to review this work.

Sincerely,
Evgeny Lazarenko

Contents

List of Figures

List of Tables

ABSTRACT

Directional Normalized Energy Stability Margin and Non-Tumbling Gait for Robust Legged Locomotion

Evgeny Lazarenko
Dept. of Mechanical and Aerospace Engineering
Graduate School of Engineering, Tokyo Institute of Technology, Tokyo, Japan

Multi-legged locomotion has always been an attractive research domain for robotics scientists. Not only because of the challenge to create machines that closely resemble living animals, but also because of significant advantages of legged locomotion over wheeled one.

A great part of work on walking robots was focused on improving their stability. This includes research on stability margins, as well as improved ways of motion control in order to increase robustness of motion.

This thesis focuses on the theory of stability. It proposes and discusses a new criterion for quantitative estimation of stability of multi-legged locomotion, called Directional Normalized Energy Stability Margin. Advantages of the criterion are discussed and examined with consideration about previous research and existing alternative stability criteria. New criterion is validated through a simulation and a tumbling experiment.

Practical application of Directional Normalized Energy Stability Margin for both static and dynamic gaits is suggested through Non-Tumbling Gait, a gait that prevents complete overturning of a robot and maintains a standing posture even when a certain disturbing force is applied to robots body from any direction.

Usage of DNESM is illustrated through examining the locomotion stability of Titan-XIII, a recently designed four-legged walking robot. Future improvements to the research are proposed and briefly discussed.

Key words : Directional Normalized Energy Stability Margin, Walking Robot, Quadruped, Legged Locomotion, Non-Tumbling Gait, Stability Margin

Chapter 1

Introduction

1.1 Brief History of Multi-legged Robots

For centuries nature has been an inspiration for makers, tinkerers, and engineers. Millions of years of evolution have forged the shapes and forms of organisms inhabiting our planet into perfect fits for Earth's ecosystems. Naturally, scientists and engineers, who witnessed all variety and functional perfection of living organisms, were lured into trying to imitate them and create artificial devices that would in one way or another repeat either behavior or structure of animals.

This fascination with nature was reflected even in ancient Greek myths, such as the myth about Deadalus who, according to the legend, was trying to fly with the help of artificial wings.

After the end of the dark ages, heritage left by Leonardo Da Vinci: his drawings and mechanical designs sparked an interest in hudnreds of artists and engineers who wanted to create something resembling life. They started building so-called "automatons", non-electronic self-operating machines (Fig. 1.1).

Legends and historical anecdotes aside, engineers kept using the benefits of natural design in their creations in our modern technological history as well. Especially this is true for mobile vehicles. Most of our planet's surface is covered with obstacles that make conventional wheeled vehicles ineffective (e.g. ravines, large rocks, slopes, and loose soil); the same is true for other bodies in our solar system. Thus, vehicles with legs are most suitable for natural terrains.

Legged vehicles were first mentioned in scientific literature in the end of the 19th century in works of Russian mathematician P. L. Chebyshev (Fig. 1.2). In

Figure 1.1: Automaton trumpet player, created by Friedrich Kaufman, ca. 1810.

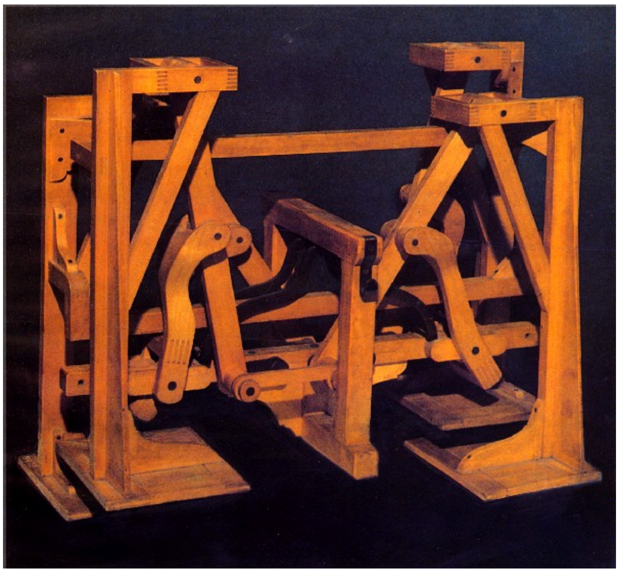

Figure 1.2: Chebyshev walking platform, 1850.

his work he tried to mimic natural walking through employing a certain four-bar mechanism.

However, actual development of legged vehicles requires solving complex problems in kinematics and dynamics. Therefore, only in the mid-20th century the science of multi-legged locomotion started to gain significant traction. First major works on walking machines date to 1940s, and focused on military legged robots. By 1970s the research on multi-legged robots was going in all major universities in the US, Japan, and Europe.

Table 1.1: Milestones in development of multi-legged vehicles.

Year	Researcher(s)	Milestone
1850	Chebyshev	Design of the linkage mechanisms used in early walking machines.
1872	Muybridge	First use of stop-motion photography to document the gaits of running animals.
1893	Rygg	First patents for legged robots are filed to the US Patent Office.
1945	Wallace	First patent of a legged vehicle for military application: a hopping tank with reaction wheels that provide stability.
1961	Morrison	Design and testing of the Iron Mule Train.
1963	Cannon, Higdon, Schaefer	Development of control systems for balancing single, double, and limber inverted pendulums.
1968	Frank and McGhee	Simple digital logic controls walking of Phony Pony.
1968	Mosher	GE quadruped truck climbs railroad ties under control of human operator.
1969	Bucyrus-Erie, Co.	Big Muskie, a 13,500-ton walking dragline, is used for strip mining.
1977	McGhee	Digital computer coordinates leg motions of hexapod walking machine.
1977	Gurfinkel	Hybrid computer controls hexapod walker in the USSR.
1980	Hirose and Umetani	Quadruped PV-II climbs stairs and climbs over obstacles using simple sensors. The leg mechanism simplifies control.
1980	Kato	Hydraulic biped walks with quasi-dynamic gait.
1980	Matsuoka	Mechanism balances in the plane while hopping on one leg.
1981	Miura and Shimoyama	Walking biped balances actively in three-dimensional space.

1983	Sutherland	Hexapod carries human rider. Computer, hydraulics, and human share computing task.
1983	Odetics Inc.	Self-contained hexapod ODEX I is commercially availabe.
1987	Waldron and McGhee	First demonstration of the ASV walking robot.
1989	Raibert	First quadruped to perform trotting, pacing, and bouncing gaits under dynamic control.

Since the beginning of the 20th century up until now, the number of multi-legged robots that is built around the world each year has been steadily increasing. However, an absolute majority of those machines are laboratory prototypes that are still very far from widespread commercialization. There is still a lot of research to be done until walking robots become as ubiquitous as their wheeled counterparts.

Currently, around 20% of walking robots being produced for research and other purposes are quadrupeds. There has been a lot of development in creating four-legged machines, and this thesis focuses on them as well.

1.2 Advantages and Disadvantages of Multi-legged Robots

There has been a lot of investigation on the advantages and disadvantages of legged vehicles in comparison to conventional machines (wheeled or tracked). For example, multi-legged vehicles demonstrate the following advantages.

1.2.1 Advantages of legged robots

Mobility

Being naturally omni-directional, legged vehicles demonstrate much better mobility than wheeled machines. Legged robots are capable of changing direction of motion without changing the orientation of the body. Wheeled vehicles, on contrary, must do some manuevering in order to achieve the same result.

Overcoming obstacles

A legged robot is capable of overcoming obstacles simply by stepping on them, while wheeled robots can only run over the obstacles which height constitutes no more than half of the wheel radius. As for tracked robots, although they can surpass wheeled ones, their mobility is still inferior to walking robots.

Active suspension

Suspension of legged robots is intrinsically active and adaptive to ground irregularities. A legged robot can walk on a rough terrain with the body levelled, and legs ensure smooth locomotion. In case of a wheeled robot, its body is always parallel to the ground and is forced to inline when encountering any uneven terrain.

Energy efficiency

Higher energy efficiency of legged robots was first suggested by British researchers A. C. Hutchinson and F. S. Smith in 1940 during their work on the first ever military walking machine. Their results were later confirmed through experimental work by Bekker (1960). Bekker's findings show that in case of un-

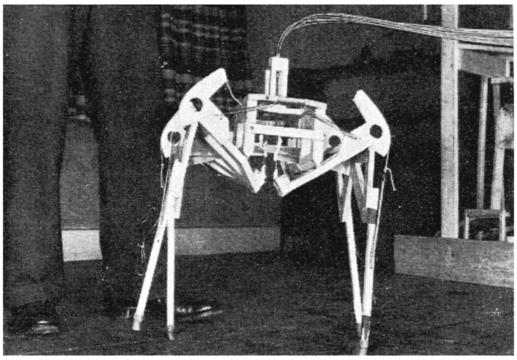

(a) Prototype of the walking tank for energy efficiency study.

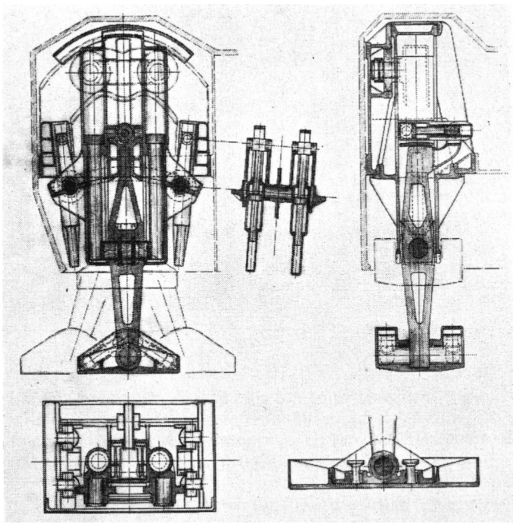

(b) Working drawing of the SuperTank

Figure 1.3: Walking SuperTank by A.C. Hutchinson and F. S. Smith., first military walking machine.

even terrain, legged robots are superior in terms of energy efficiency compared to tracked or wheeled machines.

Rough terrain locomotion

Legged robots do not require paved surfaces to move efficiently, unlike wheeled vehicles. They can move on almost any type of terrain: muddy, sandy, and rocky with almost equal efficiency. Additionally, they do not require continuos terrain to operate.

High tolerance to slipping and jamming

Wheeled robots are prone to jamming on soft or muddy terrain, which renders them incapacitated. Legs, however, do not interact with the supporting surface as much as wheels. Same is true for slipping.

Smaller environmental damage

Legged machines only need discrete ground contact points, while wheeled and tracked robots require a continuous path. This results in lower damage to the terrain which may be critical for certain exploration missions.

Higher average speed

Although it is true that wheeled and trucked vehicles can move at high speeds on prepared surfaces, when the terrain is eneven, their speed decreases significantly. Walking robots do not have such disadvantage and perform well on rocky terrain; they can maintain a similar average speed on a large variety of terrain types.

1.2.2 Disadvantages of legged robots

Although multi-legged vehicles have a wide set of advantages, they are not free of downsides. Major issues that keep walking robots from being adopted in various fields if industry are listed below.

Complex design

Wheels (or trucks, for that matter) are extremely simple devices. Wheel is essentially a rotary joint, and requires one actuator to propel it, and one – to steer. Leg, on the other hand, has multiple joints and links, and is ultimately more complex than a wheel. Electromechanical construction of legged vehicles is significantly more complex and costly than construction of wheeled machines.

Complex electronic architechture

Large number of motors required to move legged robots requires complicated electonis systems to operate them (fare more complicated than for wheeled robots).

Additional problem is the sensors for robot's actuators, as well as the amount of processing power needed to make sense of all that data in real time.

Sophisticated control algorithms

Gait control for multi-legged robots is unquestionably one of the most complicated tasks that engineers developing such robots must solve. Compared to legged robots, wheeled machines are intronsically simple, and do not require complex engineering and algorithms for coordination of the motion of wheels.

Capped maximum velocity

Higher average speed of legged robots that they can achieve on an uneven terrain has already been discussed above. However, if we compare maximum speeds that legged robots can develop on a prepared surface, it will be much lower than maximum speed of wheeled machines. For example, fast animals like horses or cheetas can achieve velocities as high as 60-80 km/h, while maximum speeds of wheeled vehicles can race up to 350 km/h and even more in some cases. Legged robots cannot (and will hardly ever be able to) compete with wheeled robots when it comes to locomotion on a flat ground.

Cost

It is well known that a cost of any system is proportional to its complexity. Being an extremely sophisticated device that requires a lot of atoms to assemble, bot literally and figuratively, even a "simple" legged robot (if there is such a thing) can cost thousands of dollars. Design and production of a wheeled robot is much less costly in comparison.

Walking robots are niche devices. They will hardly serve as a viable substitution for most wheeled machines in any forseeable future. Legged robots are only suitable (and desirable) in situations when their advantages outweight their shortcommings. Such situations can require walking on natural and otherwise uneven terrain. Next subsection discusses certain aspects of potential applicatioin of multi-legged robots.

1.3 Application of walking robots

Knowing pros and cons of legged robots, we can now deeper discuss their potential fields of application. They range from extreme robotics and operations in hazardous environments, to military applications, research, and even social and civil projects. Let us briefly discuss all of them.

1.3.1 Military use

Despite that use of military robots is ethically questionable (especially if we are talking about autonomous robots with a right to kill), walking machines can be of significant help in the field as service robots that are capable of carrying a payload on a rough, uneven, and muddy terrain.

Figure 1.4: BigDog by Boston Dynamics.

Most famous example of such military walking robot is Big Dog (Fig. 1.4) developed by Boston Dynbamics and its founder Mark Raibert.

Also, legged robots can be useful for safe operation on the minefield due to their capability to overcome obstacles.

1.3.2 Maintenance of facilities

Due to specifics of their construction, walking robots can easily operate inside buildings that are not equipped for wheeled robots (e.g., have numerous pipes on the floor, stairs, etc.). An example of such facility is a nuclear power plant.

1.3.3 Hazardous environments and dangerous operations

Planetary exploration

Although nuclear power stations can be concidered hazardous environments, there exist far more less friendly locations, such as Solar System bodies. Some interesting walking robots for planetary exploration are being designed at NASA's Jet Propulsion Laboratory. Robotic platform Athlete is, probably, the most notable example. It features a hybrid design: Athlete is a hexapod that has wheels on the ends of its legs (Fig. 1.5).

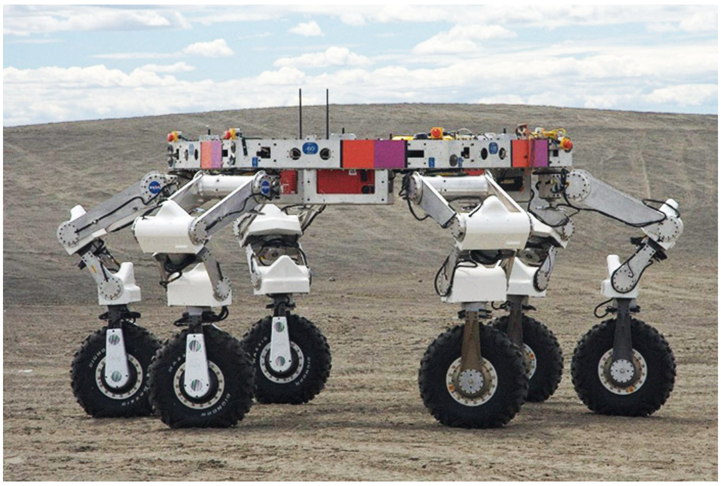

Figure 1.5: Wheeled hexapod platform Athlete by NASA JPL.

Walking robots can also perform well in exploration mission on Earth. In fact, roughy 50% of the surface of our planet is not accessible for wheeled vehicles and must be explored by using animals, robots, or from above.

Demining

It is unquestionable that humanitarian demining is a work that not only saves lives, but also improves economic development of some of the World's poorest regions. It is an expensive procedure that requires highly-skilled personnel. However, by only employing a manpower it is impossible to achieve any reasonable mine-clearance speeds. In such situation, robots seem to be the best solution for this problem.

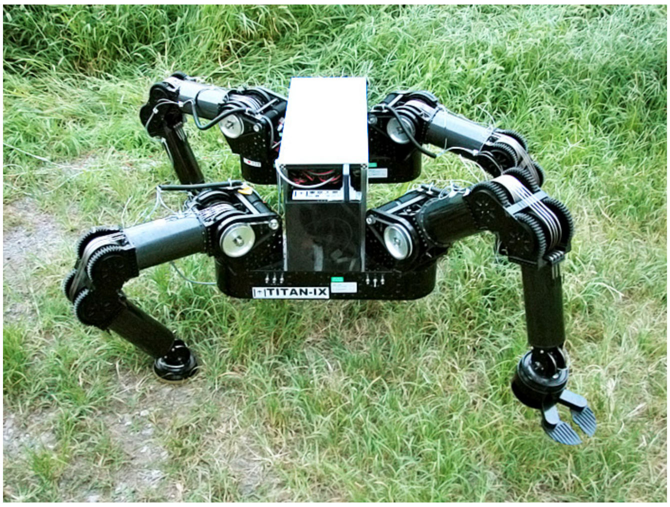

Figure 1.6: Titan-IX walking robot demonstrating one of the legs equiped with a mine unearthing tool.

Application of walking robots for demining has already been tested by Hirose and Kato, 1998 with Titan-IX robot (Fig. 1.6).

1.3.4 Forestry

Some of the less obvious fields of possible application of multi-legged robots are lumbering and agriculture. In case of lumbering works, legged machines can be successfully used in the forest where obstacles like cut tree trunks often add to a natural unevennes of the terrain (e.g. small hills or slopes). Wheeled robots are extremely difficult to use in the forest, as they require special preparation of the working terrain. One of the most notable examples of lumbering robots is a hexapod developed by Timberjack (Fig. 1.8).

Figure 1.7: Close up view of Titan-IX's end-effector.

Figure 1.8: Logging hexapod by Timberjack.

A list of applications described above does not aim to be the most comprehensive. But it clearly shows that walking robots can make a lot of difference in the way people do things. Therefore, research on them should be considered just as important as research on other types of robots.

1.4 Previous research on stability of multi-legged robots

Researchers started tackling the problem of stability of walking robots in 1960s. At that time, McGhee and Frank proposed a concept of static stability margin for an ideal walking robot. Ultimately, they defined a robot as statically stable if a projection of its center of gravity (CG) on a horizontal plane lies inside robot's supporting polygon. Although this simple criterion had a lot of limitations, this idea sparked a lot of discussion in the field of multi-legged stability.

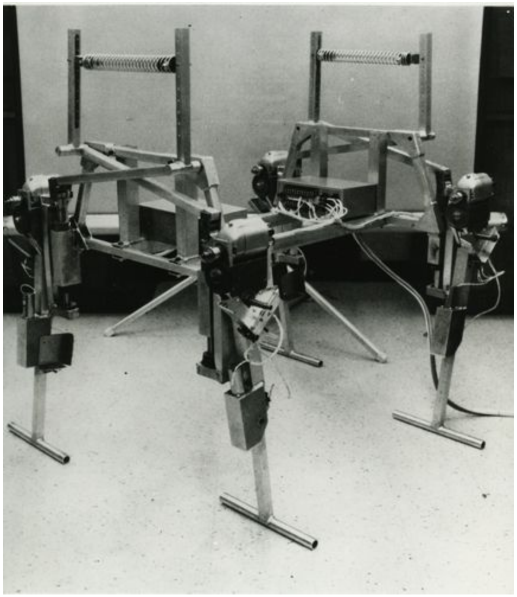

Figure 1.9: Phony Pony, a walking machine developed by McGhee and Frank in 1968.

Generally speaking, proposition made by McGhee and Frank was inspired by insects. All insects have six legs, and to propell their bodies they usually employ crawling gaits that help to maintain static stability. Similar way of locomotion has been copied by researchers lots of times, mainly because of an extremely simple gait control.

Static stability, just as the name implies, does not account for inertial effects and any other dynamic parameters (such as compliance, friction, elasticity, etc.) that occur during robots motion.

However, tremendous complexity of dynamics of multi-legged robots is a sig-

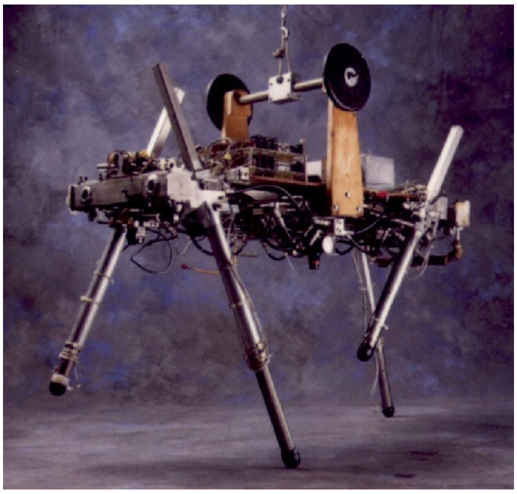

Figure 1.10: Quadruped developed by M. Raibert. The machine features hopping legs to simplify design and control.

nificant obstacle to research in dynamic stability. This forced some researchers to pursue simplifications in robot design by, for example, studying machines with only a few degrees of freedom.

Multi-legged locomotion stability is still a relatively young field, and a lot remains to be done in order to improve the understanding of stable and robust locomotion of legged robots. I hope that my work can help to improve the situation.

1.4.1 Static Stability Margin

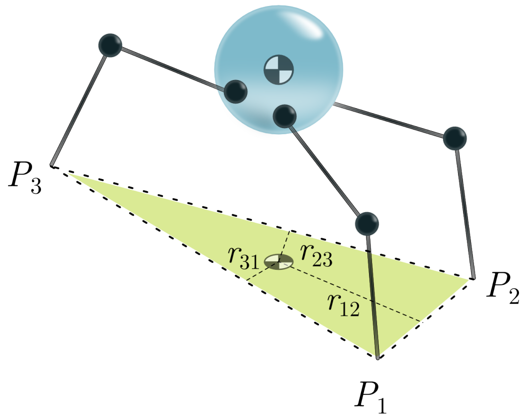

Figure 1.11: Generalized conception of Static Stability Margin as proposed by McGhee and Frank.

As it was stated above, stability-driven approach to multi-legged locomotion was suggested by McGhee and Frank in 1968 in a theorem that described a criterion which later evolved into Static Stability Margin, or SSM.

"An ideal legged locomotion machine supported by a stationary horizontal plane surface is statically stable at time t if and only if the vertical projection of the center of gravity of the machine onto the supporting surface lies within its support pattern at the given time"[7].

Albeit such theorem provided a necessary and sufficient condition to ensure the stability of an ideal walking robot, a real-life vehicle would always experience the influence of various dynamic effects and disturbances for which the theorem does not account. With that in mind, McGhee and Frank proposed SSM which indicates the ability of a vehicle to withstand external disturbances.

Thus, the definition of SSM is as follows: "the magnitude of the *static stability margin* at time t for an arbitrary support pattern is equal to the shortest distance from the vertical projection of the center of gravity to any point on the boundary of the support pattern. If the pattern is statically stable, the stability margin is positive. Otherwise, it is negative."

If S_{static} is positive, it can be calculated as

$$S_{static} = min(r_{12}, r_{23}, r_{31}), \tag{1.1}$$

where $r_{i,j}$ are the distances from robot's CG to the rotation axes (Fig. 1.11).

SSM laid the foundations of stability-driven approach to legged locomotion, and, being limited in terms of real-life applicability, fueled subsequent researches in the field.

1.4.2 Energy Stability Margin

Energy Stability Margin was proposed by Messuri and Klein [8] as a result of their work on so-called precision-footing operational mode for walking vehicles that provided improved motion control on a rough terrain. They realized that Static Stability Margin was only good for flat surfaces, and was not applicable for more complex types of terrain, such as slope, for example.

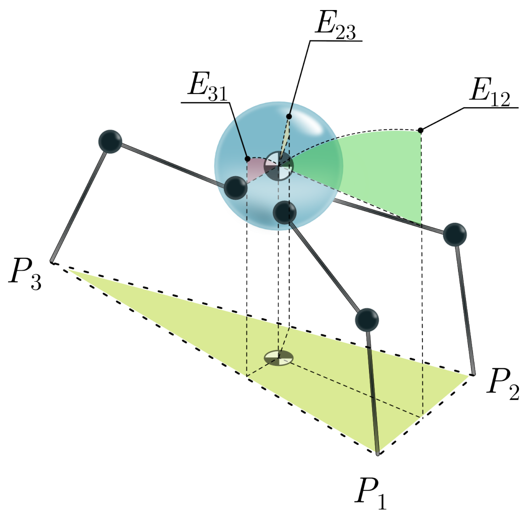

Figure 1.12: Concept of Energy Stability Margin.

This consideration resulted in the proposition of Energy Stability Margin, or ESM. This stability criterion can be formulated as the minimum potential energy, needed to overturn the robot around the edge of the supporting polygon (Fig. 1.12):

$$S_{ESM} = \overset{n_s}{\underset{i,j}{min}}(mgh_{i,j}) = min(E_{12}, E_{23}, E_{31}), \tag{1.2}$$

where mg is robot's weight, (i, j) is a pair of numbers defining neighboring footholds which form an edge of a supporting polygon representing a possible rotation axis, n_s is total number of edges of a supporting polygon, and $h_{i,j}$ is the variation of CG height at the time of its rotation around the edge of the supporting polygon.

Thus, ESM is an effective stability margin that provides qualitative estimation of the input energy that needs to be supplied to the legged vehicle system in order overturn it. It also considers the position of CG.

1.4.3 Normalized Energy Stability Margin

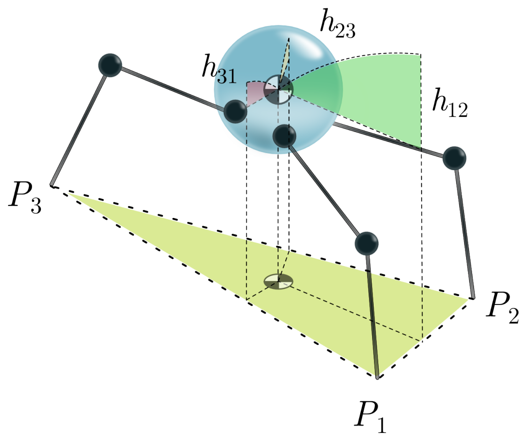

Figure 1.13: Concept of Normalized Eenergy Stability Margin for a posture with a triangle as a supporting polygon.

Although Energy Stability Margin was a fine criterion that worked well for legged locomotion on uneven terrain, it had a limitation. Namely, ESM suggested that stability of walking robots increases with their weight, even if posture does not change. Such suggestion is understandable from an energy standpoint, but it does not allow to properly compare stability between different robots.

Hirose *et al.* proposed Normalized Energy Stability Margin, or NESM, [9] that was free of such limitation. It can be represented as

$$S_{NESM} = \frac{S_{ESM}}{mg} = \overset{n_s}{\underset{i,j}{min}}(h_{i,j}), \tag{1.3}$$

or ESM normalized to robot's weight and represented by the height of a potential barrier (Fig. 1.13) to an unstable equilibrium above the edge of the supporting polygon, i.e. tumbling. Real experiments on the model of a quadruped robot standing on a slope proved that NESM is the most accurate stability margin for evaluation of stability of walking vehicles.

Not only it possesses all the advantages of ESM, but also provides a way to compare stability of different types of multi-legged robots. Moreover, NESM, is expressed in [mm], and thus can be used to empose geometric constraints on robot's gait, thus making it more stable.

1.5 Motivation for proposition of a new stability criterion

As it was explained above, through the past several decades a lot of research activity was focused on the issue of stability of legged locomotion. The majority of scholars concentrated their efforts on studying static stability of multi-legged vehicles with an assumption that stability margin can be represented by the minimum numerical value for a given supporting polygon. Speaking of direct disadvantages of previously suggested criteria, *Static Stability Margin*, for example, is only applicable for the case of flat ground, which is a highly idealized situation. It also does not account for the energy of the external disturbance required to tumble the robot. *Energy Stability Margin* does not allow to account for the effect of robot's posture on its stability, and therefore is difficult to apply in different settings. It also does not allow to compare stability of different robots.

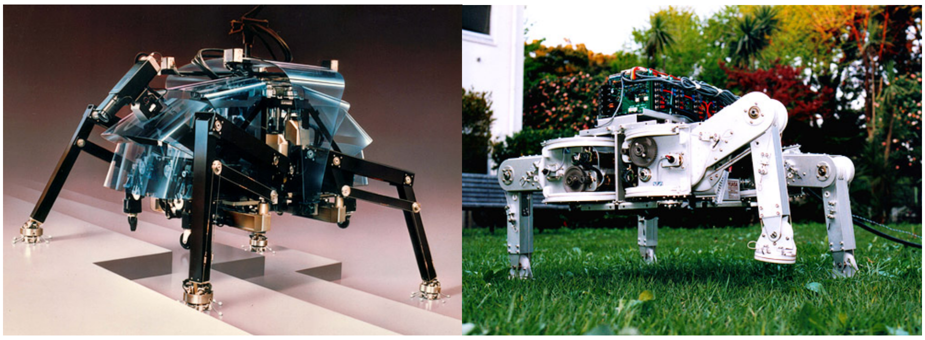

(a) TITAN IV. (b) TITAN VIII.

Figure 1.14: Examples of walking robots from Fukushima Laboratory, Tokyo Institute of Technology.

However, in course of the previous works that has been performed in Fukushima Laboratory (Tokyo Institute of Technology) on various walking robots, examples of which are presented on fig. 1.14, researchers came to the conclusion that conventional approach to stability may be improved.

Studies about the static walks were aimed on generation of an efficient terrain-adaptive leg motion sequence, while maintaining the center of gravity (CG) of the body inside the supporting polygon. There were no criteria that would deal with stability in all directions and properly consider tumbling motion and position of footholds located on a 3-dimentional uneven terrain.

This led the author to an idea that the concept of traditional Normalized Energy Stability Margin can be reworked in a way that turns it into a higlhy usable and versatile criterion which allows not only to define the stability in relation to a given edge of the supporting polygon, but also to define robot's stability in a given *direction* of external disturbance.

1.6 Structure of Thesis

This thesis proposes a new stability margin calles Directional Normalized Stability Margin, or DNESM, a new criterion that quantifies stability of multi-legged robot depending on the direction of external distubance. It further elaborates on the idea of DNESM by intoroducing a way to account for the effect that swinging leg has on locomotion stability. Finally, this thesis proposes the idea about so-called Non-Tumbling Gait and through examination of the parameters that influence DNESM, it suggests ways to generate such gait.

Chapter 1: Introduction starts with briefly outlining the history of walking machines from late XIX century until present. It also provides the information about major milestones in research on walking machines. This chapter also covers advantages (e.g. mobility, energy efficiency) and disadvantages (e.g. complex design and electronic architecture) of multi-legged robots, and then continues with discussion about their potential applications, such as military use, maintenance of facilities, and operations in hazardous environments.

Introductory chapter also discusses related former studies, giving an overview of the history of research in multi-legged stability, and then going into a more detailed discussion about three most important stability margins proposed in the previous decades, such as: Static Stability Margin, Energy Stability Margin, and Normalized Energy Stability Margin. Advantages and disadvantaged of previously suggested stability criteria are thoroughly discussed. Discussion about two most prominent disadvantages, such as lack of consideration about the direction of external disturbing energy and not accounting for the effect of robots swing leg, leads to a conclusion that a better stability margin is required.

Chapter 2: Directional Normalized Energy Stability Margin discusses the concept of DNESM in depth. Specifically, it starts with outlining the ideas which led to suggestion of DNESM, and then defines DNESM as he minimum amount of input energy E_i applied in the form of horizontal force with a yaw angular direction θ required to tumble an object, divided by the weight mg of the object itself. This chapter then provides a detailed process of derivation of Directional Normalized Energy Stability Margin through a simplified model of a robot having an arbitrary posture. Finally, this chapter discusses the validation of DNESM by means of a tumbling experiment and a numerical simulation for two different cases: flat ground and inclined surface. Experimental process was done to measure the lowest height of the pendulum that defined a corresponding potential energy required to overturn the body around the edge of a secondary supporting polygon. After several iterations for each angular position, it was possible to make a measurement of DNESM. The experiment demonstrated that the concept of DNESM and assumptions of the derivation are valid.

Proposed criterion inherits the usability and benefits of Normalized Energy Stability Margin, acting as a measure of margin length and accounting for parameters of robot's motion, and equips us with a method of more precise stability estimation, showing that multi-legged vehicles stability is not just a level of minimum energy required to overturn the robot, but a level of minimum energy applied in a certain direction, that may overturn the robot around the edge of an existing supporting polygon, or a new polygon formed by supporting legs and the swinging leg.

Chapter 3: Non-Tumbling Gait, suggests a Non-Tumbling Gait, a motion control principle that elaborates on the idea of Directional Normalized Energy Stability Margin. The idea of Non-Tumbling Gait (or NT Gait) stems from the consideration about the influence of swinging leg on locomotion stability. Its definition is based on the idea about two types of tumbling: partial and complete. Complete tumbling is a state when robot tumbles until its body hits the ground, whereas partial tumbling is a state when robot inclines, but not does not overturn due to the effect of the swing legs which hits the ground and helps to maintain standing posture. Non-Tumbling Gait is defined as a gait that prevents complete tumbling of a robot, and maintains a standing posture even when a certain disturbing force is applied to robot's body from any direction. The problem of generation of Non-Tumbling Gait is solved by extension and generalization of DNESM through consideration about the effect of the swinging leg on locomotion stability.

Chapter 4 : Validation of Generalized DNESM for Non-Tumbling Gait, discusses validation of generalized DNESM which is performed with the help of a tumbling experiment and its simulation. It also discusses practical application of DNESM and Non-Tumbling Gait, which is studied through the simulation based on Titan-XIII walking robot currently being developed at Fukushima Laboratory, Tokyo Institute of Technology. The goal of this simulation was to study parameters of motion that influence stability of the robot, as well as to find the best posture for one particular gait, and then define ways to improve the gait, thus creating a Non-Tumbling gait for a particular robot. Such simulation allowed to calculate DNESM in all stages of motion for all edges of all possible supporting polygons, and then generate a posture stability map, a simple representation of safe and unsafe postures and footholds for Titan-XIII.

This chapter also describes a tumbling experiment which was also done with Titan-XIII. The robot was performing a trot gait on a flat surface with a relatively narrow and easy to tumble posture. During motion Titan-XIII was suddenly stopped. The energy from robot's velocity was then compared to energy required to cross DNESM. If stability margin was not sufficient, the vehicle would be forced to tumble under the influence of it's own inertial factors.

An arbitrary phase of motion was chosen for the moment of a sudden stop. Robot's velocity at that point was measured, and DNESM at that point was calculated for two cases of the swing leg height: 50 mm and 15 mm. A tumbling threshold of a swing leg height was defined. Theoretical result suggested that at 0.15 step phase, robot would tumble if a swing leg height was more than 37 mm. Practical experiment showed that, in this case, actual threshold swing leg height is 30 mm. Such result is the consequence of one or a combination of intrinsic effects: compliance, slipping, and large error in the control system of the robot.

Chapter 5: Conclusions and Future Work summarizes the contents of this thesis and then suggests ways to further investigate real-life application of both Directional Normalized Energy Stability Margin and Non-Tumbling Gait. Specifically, it discusses issues that should be addressed for successful experiments with real-life robots (e.g., installing sensors, obtaining feedback about the actual state of the machine). It also suggests topics which must be studied before adoption of Directional Normalized Stability Margin becomes possible, such as: the influence of dynamic effects on DNESM (slipping and friction, inertial effects, moments in the joints, etc.), ways to adjust robots posture in order to improve DNESM during motion (e.g. by using methods of optimal control theory, or even fuzzy logic and control systems based on neural networks).

Chapter 2

Directional Normalized Energy Stability Margin

2.1 Directional Normalized Energy Stability Margin

2.1.1 Definition of DNESM

If we carefully consider destabilized motion of walking robot's CG, we can see that it always occurs in presence of a certain external force applied to robot. Obviously, that force has a direction, although in previous formulations of stability criteria, the direction of that supplied force was not explicitly considered.

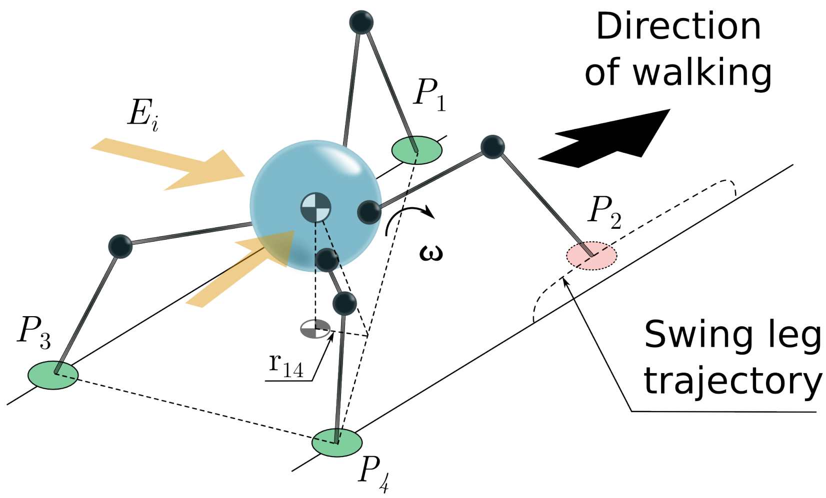

Figure 2.1: Quadruped performing trotting gait under the influence of an input energy E_i which can be directed under different angles.

Based on that idea, it is possible to propose Directional Normalized Energy

Stability Margin (DNESM), or S_θ, defined as the minimum amount of input energy E_i applied in the form of horizontal force with a yaw angular direction θ required to tumble an object, divided by the weight mg of the object itself. Proposed DNESM S_θ is expressed as follows:

$$S_\theta = \left.\frac{E_i}{mg}\right|_\theta . \tag{2.1}$$

In this criterion it is assumed that the phenomenon of instanteneous time occurs, and robot's movement is measured in descreete time snapshots. Therefore, even though the velocity $\mathbf{V}(E_i)$ is created by a certain input force which is, in turn, caused by an input energy E_i, we may neglect such parameters as acceleration under the influence of that force, feet slipping, etc. Input energy E_i is applied to the center of gravity of the object in the form of force $\mathbf{F}(E_i)$ that acts in the horizontal plane on the yaw angle θ and generates velocity $\mathbf{V}(E_i)$.

It is also assumed that the application of input energy E_i to the object is done at a time t while CG of the object is making a motion with velocity $\mathbf{V}_b$ and angular velocity $\boldsymbol{\omega}_b$, and as soon as input energy E_i is applied, the internal motion of the object is frozen and the object starts a new motion with velocity $\mathbf{V}_b + \mathbf{V}(E_i)$ and angular velocity $\boldsymbol{\omega}_b$.

As the dimension of the stability criterion S_θ is "length", it can be considered to be the height of potential barrier of the object formed to the horizontal direction θ against input disturbance energy.

Proposed Directional Normalized Energy Stability Margin, or S_θ, inherits the usability and benefits of Normalized Energy Stability Margin, acting as a measure of margin length and accounting for parameters of robot's motion, and equips us with a method of more precise stability estimation, showing that multilegged vehicles' stability is not just a level of minimum energy required to overturn the robot, but a level of minimum energy applied in a certain direction, that may overturn the robot around the edge of an existing supporting polygon, or a new polygon formed by supporting legs and the swinging leg.

2.2 Derivation of DNESM

2.2.1 Tumbling Motion Analysis

To clarify the derivation process, let us analyze tumbling motion of a walking robot. This chapter will only consider the case of an n-legged supporting polygon, and will not account for the effect of the swinging legs. This is done for the simplification of the derivation. Tumbling-prevention, including the effect of the swinging legs, will be discussed in the following chapters.

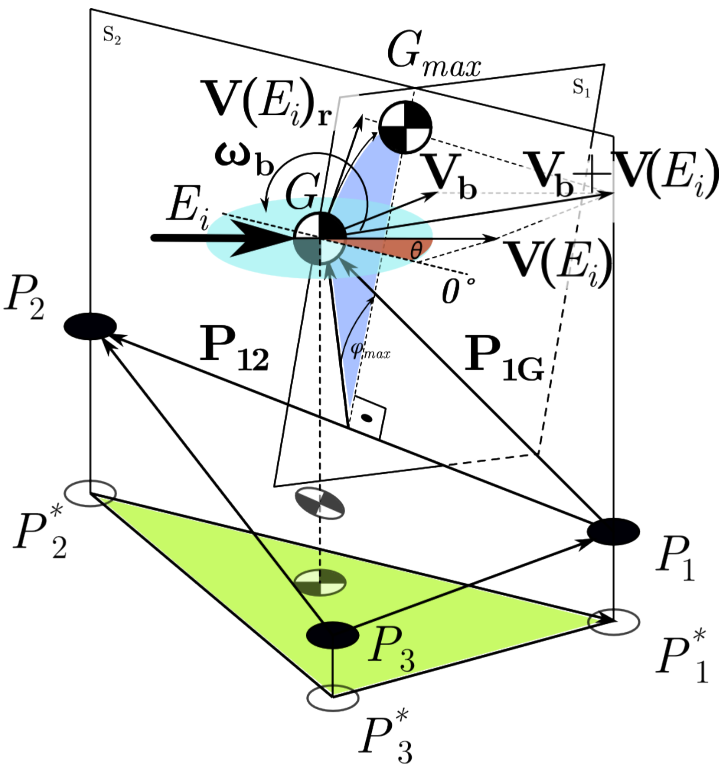

Figure 2.2: CG rotation around the edge of the supporting polygon. S_1 is the plane of CG rotation around P_1P_2, and S_2 is a vertical plane of an unstable equilibrium above P_1P_2. Other variables are defined below.

Let us consider the simplest case of a 3 leg supported walking robot with no swinging legs, and its movement in presence of a certain input energy E_i that is applied in the form of horizontal input velocity $\mathbf{V}(E_i)$ of the CG (Fig. 2.2). P_1, P_2, P_3 are ground contact points, while P_1^*, P_2^*, P_3^* are their projections on a horizontal plane.

Destabilizing energy E_i is supplied to the system in order to overturn the robot. Main condition for overturning is moving robot's CG from its current stable position G to a position G_{max} – an unstable equilibrium in rotation around P_1P_2 axis.

In order to derive S_θ, let us consider the case when robot's CG experiences a rotation around P_1P_2 line (figure 2.2), produced by means of an externally applied input velocity $\mathbf{V}(E_i)$ lying in a horizontal plane. Yaw direction θ of $\mathbf{V}(E_i)$ is variable, and its magnitude is defined by the amount of energy required to overturn the robot.

Let us define all necessary variables and derive $\mathbf{V}(E_i)$ magnitude, as shown on Fig. 2.2. First, we shall derive the rotational velocity $\mathbf{V}(E_i)_r$ generated by the input velocity $\mathbf{V}(E_i)$.

Footholds of the supporting polygon and CG of the robot may be written as $P_i(x_i, y_i, z_i), i = 1 \ldots 3$, and $G(x_G, y_G, z_G)$.

Vector $\mathbf{P}_{12}$ from P_1 to P_2 is expressed as

$$\mathbf{P}_{12} = (x_2 - x_1, y_2 - y_1, z_2 - z_1)^T, \tag{2.2}$$

and its unit vector $\hat{\mathbf{P}}_{12}$:

$$\hat{\mathbf{P}}_{12} = \frac{1}{\sqrt{(x_2 - x_1)^2 + (y_2 - y_1)^2 + (z_2 - z_1)^2}} \begin{bmatrix} x_2 - x_1 \\ y_2 - y_1 \\ z_2 - z_1 \end{bmatrix}. \tag{2.3}$$

Vector $\mathbf{P}_{1G}$ from P_1 to G is expressed as

$$\mathbf{P}_{1G} = (x_G - x_1, y_G - y_1, z_G - z_1)^T, \tag{2.4}$$

and its unit vector $\hat{\mathbf{P}}_{1G}$ is expressed as

$$\hat{\mathbf{P}}_{1G} = \frac{1}{\sqrt{(x_G - x_1)^2 + (y_G - y_1)^2 + (z_G - z_1)^2}} \begin{bmatrix} x_G - x_1 \\ y_G - y_1 \\ z_G - z_1 \end{bmatrix}. \tag{2.5}$$

The unit vector $\hat{\mathbf{V}}_{12G}$ of transverse velocity of CG's rotation around $\mathbf{P}_{12}$ can be written as:

$$\hat{\mathbf{V}}_{12G} = \hat{\mathbf{P}}_{12} \times \hat{\mathbf{P}}_{1G}, \tag{2.6}$$

$$\hat{\mathbf{V}}_{12G} = \frac{1}{\|\mathbf{P}_{12} \times \mathbf{P}_{1G}\|} \begin{vmatrix} i & j & k \\ x_2 - x_1 & y_2 - y_1 & z_2 - z_1 \\ x_G - x_1 & y_G - y_1 & z_G - z_1 \end{vmatrix}, \tag{2.7}$$

where i, j, k are unit vectors of the chosen cartesian coordanate frame;

$$\hat{\mathbf{V}}_{12G} = \frac{1}{\|\mathbf{P}_{12} \times \mathbf{P}_{1G}\|} \mathbf{A_{12}}, \tag{2.8}$$

where

$$\mathbf{A_{12}} = \begin{bmatrix} (y_2 - y_1)(z_G - z_1) - (y_G - y_1)(z_2 - z_1) \\ -(x_2 - x_1)(z_G - z_1) + (x_G - x_1)(z_2 - z_1) \\ (x_2 - x_1)(y_G - y_1) - (x_G - x_1)(y_2 - y_1) \end{bmatrix}. \tag{2.9}$$

At the same time, let us express horizontal input velocity as

$$\mathbf{V}(E_i) = (V(E_i)\cos\theta, V(E_i)\sin\theta, 0)^T. \tag{2.10}$$

Then, rotational velocity $\mathbf{V}(E_i)_r$ of the CG around vector $\mathbf{P}_{12}$ caused by the input velocity $\mathbf{V}(E_i)$ can be expressed as

$$\mathbf{V}(E_i)_r = \big(\mathbf{V}(E_i) \cdot \hat{\mathbf{V}}_{12G}\big)\hat{\mathbf{V}}_{12G}, \tag{2.11}$$

By substituting equations (2.8) and (2.10) parameters of equation (2.11) can be expressed as

$$\mathbf{V}(E_i) \cdot \hat{\mathbf{V}}_{12G} = \frac{V(E_i)B_{12}}{\|\mathbf{P}_{12} \times \mathbf{P}_{1G}\|}, \tag{2.12}$$

where

$$\begin{aligned} B_{12} = \Big[&\big((y_2 - y_1)(z_G - z_1) - (y_G - y_1)(z_2 - z_1)\big)\cos\theta \\ &+ \big(-(x_2 - x_1)(z_G - z_1) + (x_G - x_1)(z_2 - z_1)\big)\sin\theta\Big]. \end{aligned} \tag{2.13}$$

Therefore, rotational velocity of CG generated by the input velocity $\mathbf{V}(E_i)$ can be expressed as

$$\mathbf{V}(E_i)_r = \frac{V(E_i)B_{12}}{\|\mathbf{P}_{12} \times \mathbf{P}_{1G}\|^2} \mathbf{A_{12}}. \tag{2.14}$$

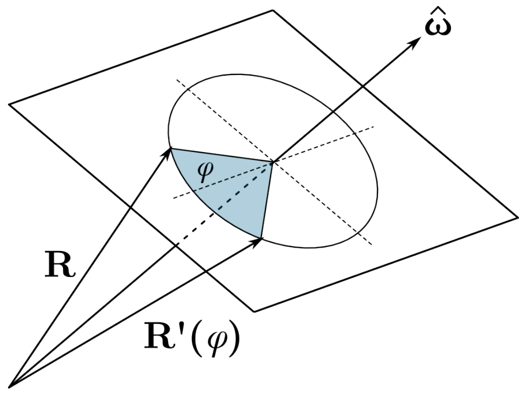

Figure 2.3: Vector rotation.

Next, we have to define a top point G_{max} which CG can reach in its rotation around $\mathbf{P}_{12}$, the point of maximum potential energy and unstable equilibrium above P_1P_2 edge. It is known that rotated vector $\mathbf{R}$ around vector $\hat{\boldsymbol{\omega}}$ on angle φ (Fig. 2.3) can be expressed as

$$\mathbf{R}'(\varphi) = (\mathbf{R} \cdot \hat{\boldsymbol{\omega}})\hat{\boldsymbol{\omega}} + \cos\varphi(\mathbf{R} - (\mathbf{R} \cdot \hat{\boldsymbol{\omega}})\hat{\boldsymbol{\omega}}) + \sin\varphi(\hat{\boldsymbol{\omega}} \times \mathbf{R}). \tag{2.15}$$

This relation can be used to describe our case in a similar fashion by substituting $\mathbf{P}_{1G}$ as $\mathbf{R}$, $\hat{\mathbf{P}}_{12}$ as $\hat{\boldsymbol{\omega}}$, and vector $\mathbf{P_{1G}}(\varphi) = \mathbf{G}(\varphi) - \mathbf{P_1}$ as $\mathbf{R}'(\varphi)$, giving us the following equation:

$$\begin{aligned} \mathbf{G}(\varphi) = {} & (\mathbf{P}_{1G} \cdot \hat{\mathbf{P}}_{12})\hat{\mathbf{P}}_{12} + \cos\varphi\big(\mathbf{P}_{1G} - (\mathbf{P}_{1G} \cdot \hat{\mathbf{P}}_{12})\hat{\mathbf{P}}_{12}\big) + \\ & + \sin\varphi(\hat{\mathbf{P}}_{12} \times \mathbf{P}_{1G}) + \mathbf{P_1}. \end{aligned} \tag{2.16}$$

Here, $\mathbf{P}_{1G} \cdot \hat{\mathbf{P}}_{12}$ can be expressed from equations (2.3) and (2.4) as

$$\mathbf{P}_{1G} \cdot \hat{\mathbf{P}}_{12} = \frac{1}{\|\mathbf{P}_{12}\|} C_{12}, \tag{2.17}$$

where

$$C_{12} = (x_G - x_1)(x_2 - x_1) + (y_G - y_1)(y_2 - y_1) + (z_G - z_1)(z_2 - z_1). \tag{2.18}$$

And $\hat{\mathbf{P}}_{12} \times \mathbf{P}_{1G}$ is expressed from equations (2.6) and (2.8) as:

$$\hat{\mathbf{P}}_{12} \times \mathbf{P}_{1G} = \frac{1}{\|\mathbf{P}_{12}\|}\mathbf{A_{12}}. \tag{2.19}$$

By substituting members of (2.16) with previously found relations, we can write a function defining the CG movement around P_1P_2 axis:

$$\begin{aligned}\mathbf{G}(\varphi) = \frac{C_{12}}{\|\mathbf{P}_{12}\|^2}\begin{bmatrix} x_2 - x_1 \\ y_2 - y_1 \\ z_2 - z_1 \end{bmatrix} + \\ + \cos\varphi \begin{bmatrix} (x_G - x_1) - \frac{C_{12}}{\|\mathbf{P}_{12}\|^2}(x_2 - x_1) \\ (y_G - y_1) - \frac{C_{12}}{\|\mathbf{P}_{12}\|^2}(y_2 - y_1) \\ (z_G - z_1) - \frac{C_{12}}{\|\mathbf{P}_{12}\|^2}(z_2 - z_1) \end{bmatrix} + + \frac{\sin\varphi}{\|\mathbf{P}_{12}\|}\mathbf{A_{12}} + \mathbf{P}_1,\end{aligned} \tag{2.20}$$

where $\mathbf{A_{12}}$ is shown in the equation (3.4).

Obviously, we have to find φ_{max}, the angle travelled by CG to the highest point rotation around P_1P_2. Highest position of $\mathbf{G}(\varphi)$ can be derived by the extremum of its equation of motion $\partial\mathbf{G}(\varphi)_z/\partial\varphi = 0$, where $\mathbf{G}(\varphi)_z$ is the z component of $\mathbf{G}(\varphi)$, and expressed as:

$$\begin{aligned}\frac{\partial \mathbf{G}(\varphi)_z}{\partial\varphi} = -\sin\varphi_{max}\Big(z_G - z_1 - \frac{C_{12}}{\|\mathbf{P}_{12}\|^2}(z_2 - z_1)\Big) \\ + \frac{\cos\varphi_{max}}{\|\mathbf{P}_{12}\|}\Big((x_2 - x_1)(y_G - y_1) - (x_G - x_1)(y_2 - y_1)\Big) = 0.\end{aligned} \tag{2.21}$$

thus, the following equation holds:

$$\frac{\sin\varphi_{max}}{\cos\varphi_{max}} = D_{12}, \tag{2.22}$$

where

$$D_{12} = \frac{(x_2 - x_1)(y_G - y_1) - (x_G - x_1)(y_2 - y_1)}{\|\mathbf{P}_{12}\|(z_G - z_1) - \frac{C_{12}}{\|\mathbf{P}_{12}\|}(z_2 - z_1)}. \tag{2.23}$$

Finally, angular distance φ_{max} can be expressed as

$$\varphi_{max} = \arctan(D_{12}). \tag{2.24}$$

From (3.6) and (2.16) we can define $\mathbf{G}_{max}$ as $\mathbf{G}(\varphi_{max})$, and it is expressed as

$$\begin{aligned}\mathbf{G}_{max} = \frac{C_{12}}{\|\mathbf{P}_{12}\|}\hat{\mathbf{P}}_{12} + \cos\varphi_{max}\Big(\mathbf{P}_{1G} - \frac{C_{12}}{\|\mathbf{P}_{12}\|}\hat{\mathbf{P}}_{12}\Big) + \\ + \sin\varphi_{max}\frac{\mathbf{A_{12}}}{\|\mathbf{P}_{12}\|} + \mathbf{P_1}.\end{aligned} \tag{2.25}$$

Height difference between original CG position G and the highest position of G_{max} can be expressed as

$$H_{12} = G_{max\ z} - G_z. \tag{2.26}$$

Magnitude of $V(E_i)$ to move CG just to the top position G_{max} is

$$\frac{1}{2}m\|\mathbf{V}(E_i)_r\|^2 = mgH_{12}. \tag{2.27}$$

From (2.12):

$$\|\mathbf{V}(E_i)_r\|^2 = Z_{12}^2\mathbf{V}^2(E_i), \tag{2.28}$$

where Z_{12} is defined as

$$Z_{12}^2 = \Big(\frac{B_{12}}{\|\mathbf{P}_{12} \times \mathbf{P}_{1G}\|^2}\Big)^2\mathbf{A_{12}^T}\mathbf{A_{12}}. \tag{2.29}$$

As a result, input velocity $V(E_i)$ needed to move CG to the top position above P_1P_2 edge can be expressed as

$$\frac{1}{2}mV^2(E_i) = mg\frac{H_{12}}{Z_{12}^2}. \tag{2.30}$$

Thus, Directional Normalized Energy Stability Margin, or S_θ, corresponding potential barrier to the input velocity in the direction θ, can be expressed as:

$$S_\theta = \frac{H_{12}}{Z_{12}^2}. \tag{2.31}$$

2.2.2 Calculation of S_θ for a generalized supporting posture

This section summarizes a calculation of S_θ for a walking robot with an arbitrary n-legged supporting posture.

Again, it is assumed that a walking robot is affected by an input energy E_i that generates horizontal input velocity $\mathbf{V}(E_i)$ of the CG (Fig. 2.2). P_i and P_j are neighbouring ground contact points.

Edges of the supporting polygon and CG of the robot may be denoted as $P_{i,j}(x_{ij}, y_{ij}, z_{ij}), i = 1 \ldots n$, and $G(x_G, y_G, z_G)$ correspondingly.

Thus, DNESM S_θ for the edge of the supporting polygon connecting i-th and j-th foothold may be easily computed through the following algorithm.

1. Find necessary coefficients $\mathbf{A_{i,j}}$, $B_{i,j}$, $C_{i,j}$, and $D_{i,j}$ from equations (3.4), (3.9), (3.5), and (3.7) correspondingly.

2. Find a maximum angular displacement of robot's CG $\varphi_{i,j}^{max}$ from equation (3.6).

3. From (3.3) calculate $G_{(i,j)max}$.

4. Calculate $H_{i,j}$, height difference between original CG position G and its highest possible position $G_{(i,j)max}$ above $(\mathbf{i}, \mathbf{j})$, from (3.2).

5. Calculate a coefficient $Z_{i,j}$ for an $(\mathbf{i}, \mathbf{j})$ axis from (3.8).

6. Finally, S_θ for an $(\mathbf{i}, \mathbf{j})$ line of supporting polygon can be calculated as

$$S_\theta = \frac{H_{i,j}}{Z_{i,j}^2}. \tag{2.32}$$

It is interesting to notice that Normalized Energy Stability Margin is, in fact, a case of Directional Normalized Energy Stability Margin. It is easy to show that in a boundary case, when input energy is directed normally to the (i, j)-th edge of the supporting polygon, S_θ is minimum for this particular edge, which is the same as NESM.

2.3 Validation of DNESM

2.3.1 Numerical simulation

Equation (2.31) which allows to calculate DNESM was derived with certain assumptions. In order to find out whether those assumptions are correct and how well the performed derivation process corresponds to a real life situation, it is required to perform a numerical simulation first, and then a model experiment with some kind of actual model of a robot, measuring S_θ manually, and comparing the results with a simulation for the same model.

In order to perform initial validation of S_θ, the author have created a numerical model for its calculation. Model was developed using MathCad, and did not account for various dynamic effects of the environment. Such limitations were introduced because relistic simulation (a simulation that would account for friction, toqrue effects in the joint actuators, etc.) was not critical for validation.

A simulation scenario can be described in the following points:

- External energy E_i is supplied to the system in a horizontal plane, and, thus, $\mathbf{V}(E_i)$ lays in the horizontal plane as well.
- In numerical simulation friction in the footholds is infinite, and slipping does not occur.
- In numerical simulation legs are massless, and robot's mass is concentrated in the body.
- Body velocity $\mathbf{V}_b = 0$ and $\boldsymbol{\omega_b} = 0$ in both cases.
- Simulation and experiment are conducted on both flat and uneven surfaces (slope).
- In numerical simulation initial position of CG corresponds with the position of CG in a physical model. However, examining the relationship between such initial condition as the position of robot's CG and S_θ is not the goal of the validation. Therefore, initial position of CG remains constant in all simulation and experiment cases.

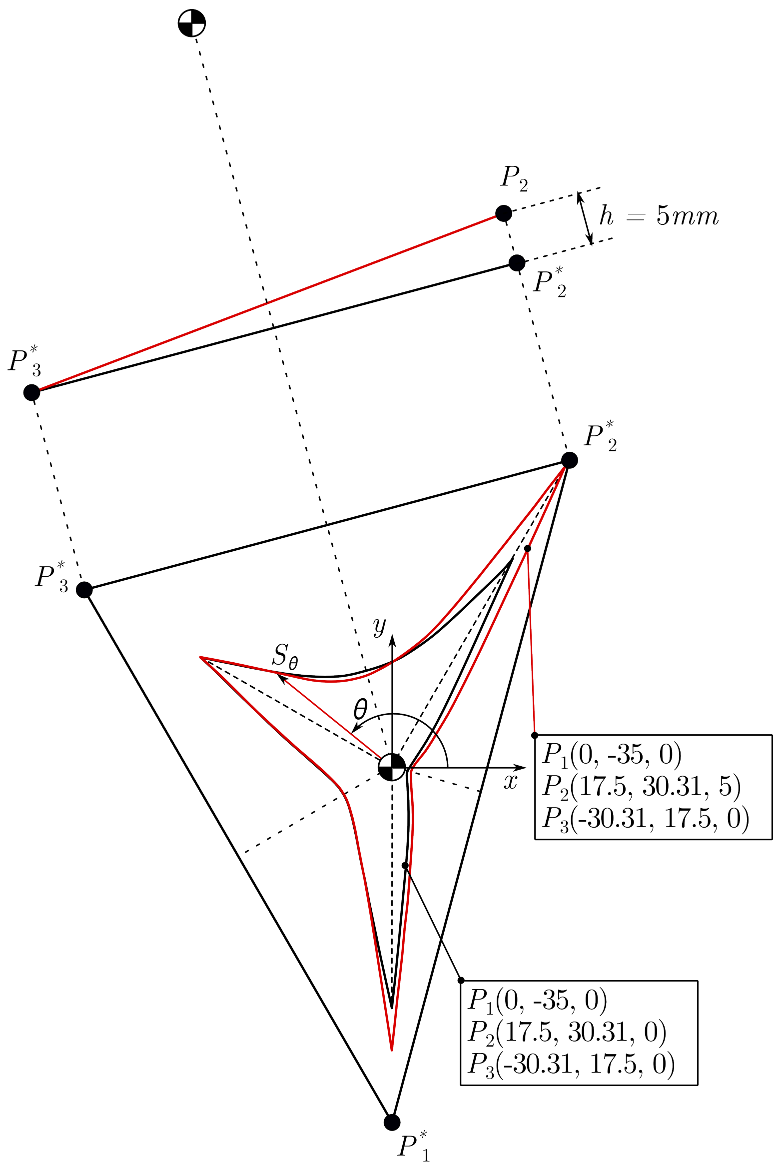

Figure 2.4: Calculation of S_θ for two cases. Numbers are the coordinates of footholds in mm, when projection of CG on a horizontal plane is in the origin of cortesian coordinate system. S_θ is plotted in polar coordinates with CG in the center of coordinate frame.

Simulation was conducted for two cases: $P_2 = (17.5, 30.31, 0)^T$ (flat ground) and $P_2 = (17.5, 30.31, 5)^T$ (slope). Results are shown on Fig. 2.4. Simulation results for flat ground are shown in black line, and results for the case of slope are shown in red.

2.3.2 Tumbling experiment

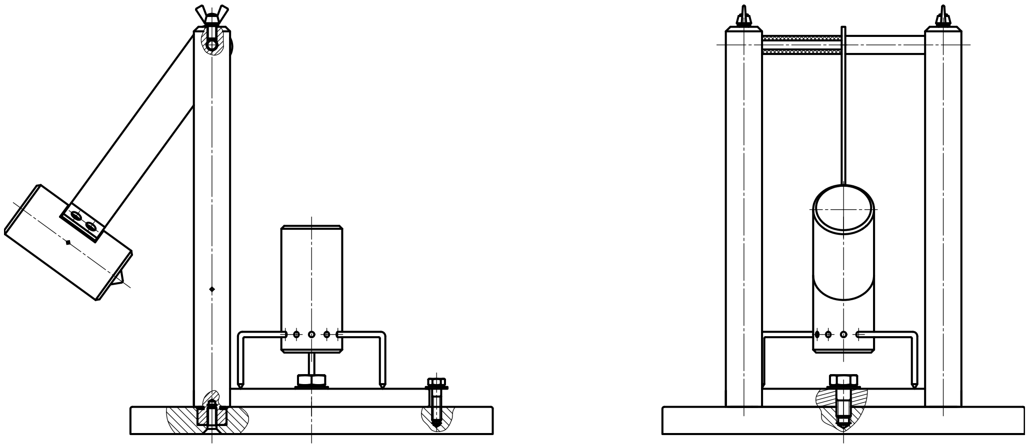

Figure 2.5: Drawing of the experimental setup.

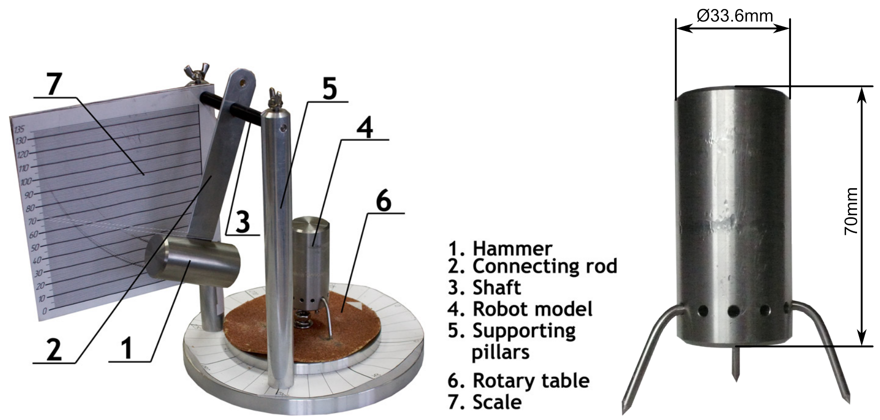

(a) Impact table. (b) Robot model 4.

Figure 2.6: Experimental setup.

In order to validate proposed derivation process of DNESM S_θ, a simple tumbling experiment with a specially designed experimental setup was performed. Setup design was done in CAD package Kompas, and two views of the assembly are shown on Fig. 2.5. Photo of the actual device is shown on Fig. 2.6.

Experimental setup consisisted of the following elements:

- Pendulum with a hammer 1 (mass: 470 g) attached to a connecting rod 2 and rotating on a shaft 3.

- Robot model 4 (mass: 490 g) with lightweight legs (mass of each leg 2.3g), Fig. 2.6b. (As mass of the legs is small compared to mass of the body, they can be neglected.)
- Supporting pillars 5.
- Rotary table 6 for positioning the body.
- Vertical scale 7 for measuring the value of S_θ.

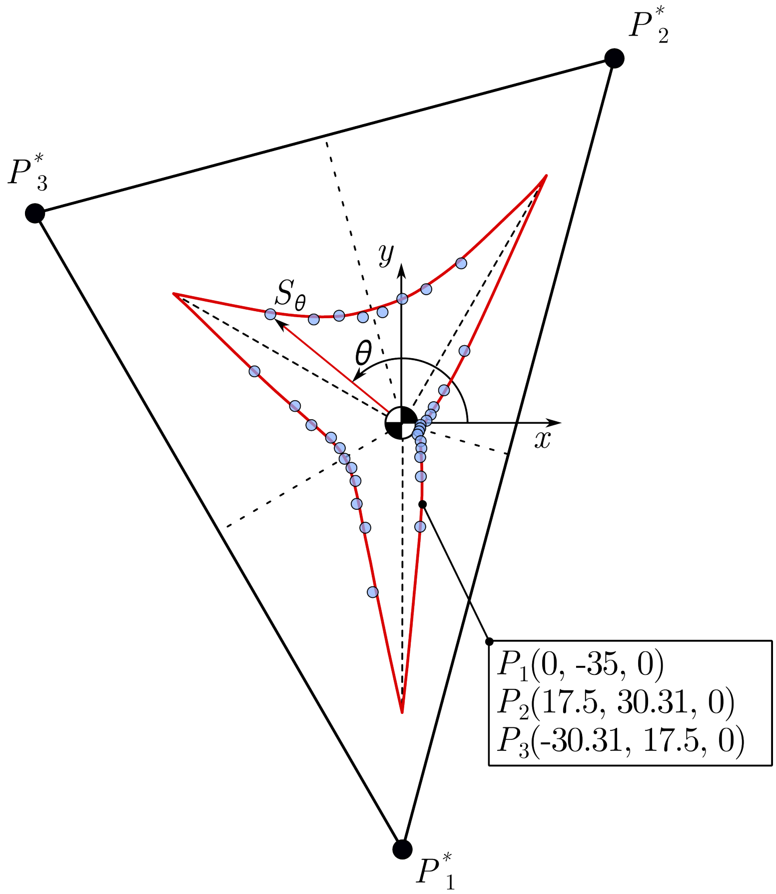

Figure 2.7: Calculation of S_θ for the case of a flat ground. Experimental results are shown as dots and derived S_θ is shown as a red line.

Experimental process was done to measure the lowest height of the pendulum that defined a corresponding potential energy required to overturn the body.

After several iterations for each angular position, it was possible to make a final measurment of S_θ with a certain precision.

One of the limiting factors of such work was insufficient friction of the surface of a rotary table of the experimental setup. In cases when S_θ was high, slipping of the body occured, which resulted in a significant lack of measurment accuracy. To solve this problem, rotary table was covered with sandpaper which greatly improved the quality of measurements.

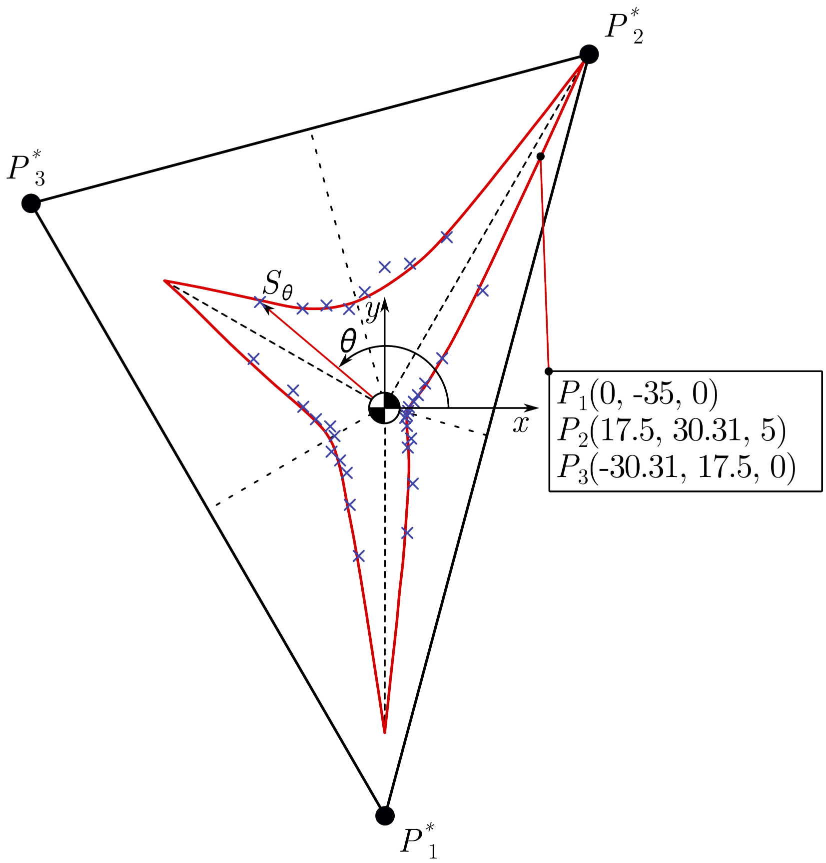

Figure 2.8: Calculation of S_θ for the case of a slope. Leg 2 height is 5 mm. Experimental results are shown as crosses and derived S_θ is shown as a red line.

Data from the simulation and experiment were compared, and are presented on Fig. 4.2.

Fig. 2.8 demonstrates a case of a slope when leg 2 foothold position is 5 mm higher, compared to the previous case.

As one can see on the graph, experimental results correspond well with the derivation results of S_θ as it was proposed above. This proves general validity of our proposed method.

Chapter 3

Non-Tumbling Gait

3.1 Introduction to Non-Tumbling Gait

This chapter will further investigate the properties and possible applications of Directional Normalized Stability Margin, or S_θ. This will be done through the duscission about the effect that swinging leg may have on the stability of a multi-legged robot during its motion.

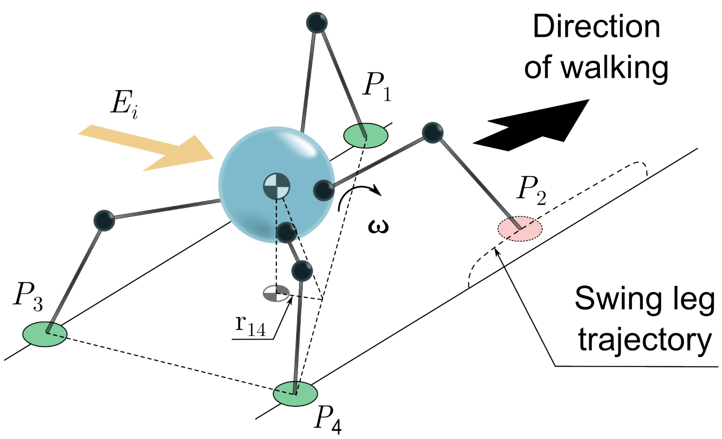

Figure 3.1: Crawling gait. E_i is an external energy supplied to the system, r_{14} is the shortest distance to P_1P_4 edge of the supporting polygon $P_1P_3P_4$.

Ultimately, all stability-related studies are aimed at generation of an efficient terrain-adaptive leg motion sequence. Most of them achieve this by maintaining the center of gravity (CG) of the body inside the supporting polygon.

For instance, posture stability in Fig. 3.3a case may be defined by the shortest distance r_{14}, connecting footholds P_1 and P_4, and gait control algorithms are

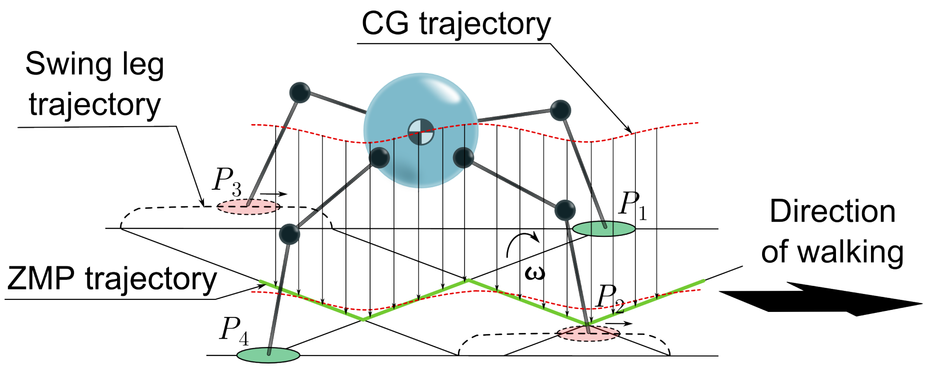

Figure 3.2: Trotting gait. CG trajectory is shown as a red dashed line, ZMP trajectory is represented by a wide bright-green line, arrows from CG trajectory show the position of ZMP at every corresponding point.

based on this condition. In case of Fig. 3.4a, it was considered that the CG of the body should follow the hyperbolic curve in order to follow a ZMP zigzag line connecting the supporting legs [11, 12].

In former studies it was also considered that once planned motion is disturbed, and the walking robot starts to tumble, it is all over, and the operation has failed. In case of Fig. 3.3a, once the CG tumbles in the direction of r_{14} and crosses P_1P_4, gait control is considered a failure. In case of dynamic walk demonstrated on Fig. 3.4a, if robot's CG cannot follow a proper hyperbolic curve because of, for example, a strong wind, walking robot starts to tumble and, unless the adjustment of next two leg supporting position is not performed, operation is failed.

However, after studing previous works that has been done in Fukushima Laboratory on various walking robots, the author came to the conclusion that researchers should always consider real-life applications and behavior of the walking robots.

In case of Fig. 3.3a, when robot tumbles in the direction of P_1P_4, swinging leg moving above the ground may contact it, and this effect may prevent complete tumbling of the robot. In case of dynamic walk (Fig. 3.4a), tumbling motion around line P_1P_4 may be prevented by the hit of a swing leg, when either P_2 or P_3 touches the ground.

Until now, such effect has never been considered in the studies of the walking robots' gait control. Thus, a further research on the matter of this effect was performed. This led to proposition of a new paradigm of gait control for future practical use of the walking robots.

As the quantitative planning of the proposing gait control needs a new type of criterion of stability, a new type of stability criterion was suggested. Such criterion takes into account dynamic effects of the tumbling motion, and also the difference of the resistance against directional disturbance force applied to a walking robot. Applicability of this stability criterion was verified by an experiment with a simple model.

3.2 Definition of Non-Tumbling Gait

When a multi-legged robot cannot maintain a planned stable walking or running due to some disturbance, e.g. wind, its movement can be described by one of the two tumbling states: complete tumbling and partial tumbling. Complete tumbing is a state when robot tumbles until its body hits the ground, whereas partial tumbling is a state when robot inclines, but not does not overturn due to the effect of the swing legs which hits the ground and helps to maintain standing posture. Fig. 3.3 and 3.4 illustrate partial tumbling in detail.

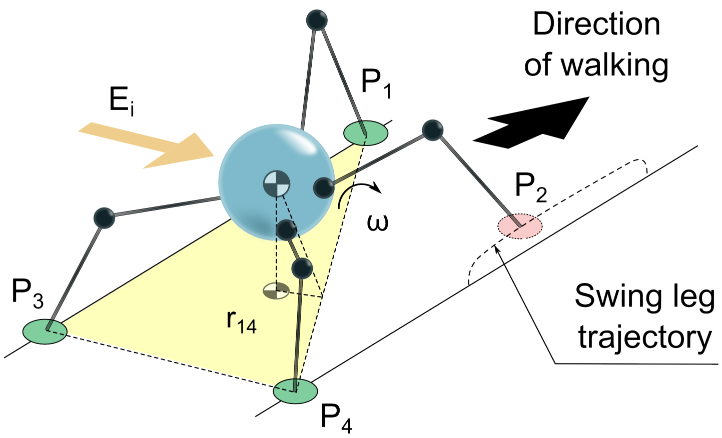

(a) Crawling gait before the application of disturbing input energy E_i.

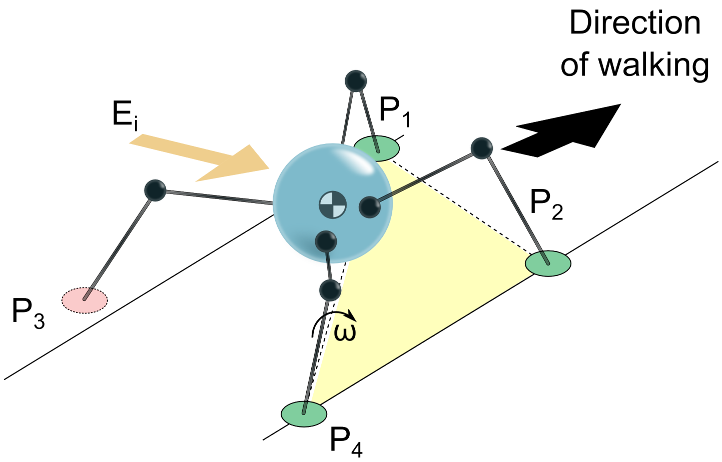

(b) Crawling gait after the application of disturbing input energy E_i.

Figure 3.3: Crawling gait and subsequent rotation after the application of external disturbing energy.

Case of crawling gait

Let us assume that the robot is performing a statically stable crawling gait and maintaining stability by forming a supporting triangle with legs P_1, P_3, and P_4. Disturbance energy E_i is applied to the body of the robot as shown in Fig. 3.3a. When disturbance energy E_i is large, robot may start tumbling around the line connecting P_1 and P_4, and the swing leg P_2 may hit the ground. If disturbance energy is very large, the robot may overturn completely. However, if it is not, robot will maintain a standing posure with a newly formed supporting polygon $P_1P_2P_4$. This latter state is what can be called a partial tumbling in a static walking.

Case of trot gait

Let us assume that the robot is preforming a dynamically stable trot gait and maintaining a planned dynamic motion while keeping the ZMP of the body on the line connecting P_1 and P_4. Disturbance energy E_i is applied as shown on Fig. 3.4a. If disturbance energy E_i is very large, the robot may tumble completely. However, if it is not, the robot will maintain a standing posure with a newly formed supporting supporting polygon $P_1P_2P_4$ in case of Fig. 3.4b, or $P_1P_2P_4$ in case of Fig. 3.4c. This latter state is what we call a partial tumbling in a dynamic walking.

Both complete and partial tumbling are, of course, not desireable, and they should be avoided. From practical viewpoint, however, partial tumbling is far more preferrable than complete tumbling, because it would not damage of the body, and resuming normal walking sequence or running in case of partial tumbling is easy. In such case, even though planned motion is disrupted and smooth locomotion cannot be maintained, robot can avoid overturning. Thus, such destabilized motion may be considered safe.

Until now, there were many discussions about the stability criteria for statically stable walking, such as: Static Stability Margin [7], Energy Stability Margin [8], Normalized Energy Stability Margin [9], and, finally, Directional Normalized Energy Stability Margin. But all of these criteria only consider the con-

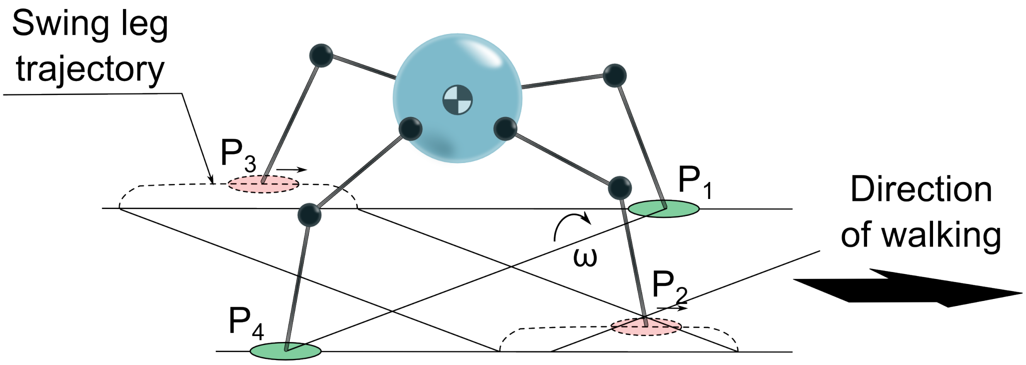

(a) Trotting gait before the application of disturbing energy.

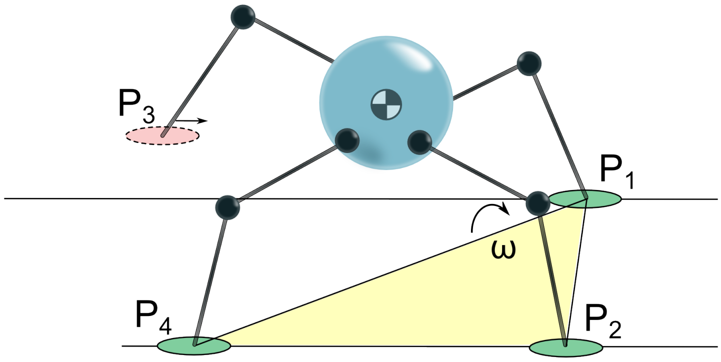

(b) Trotting gait after the application of disturbing energy, case of forward tilting.

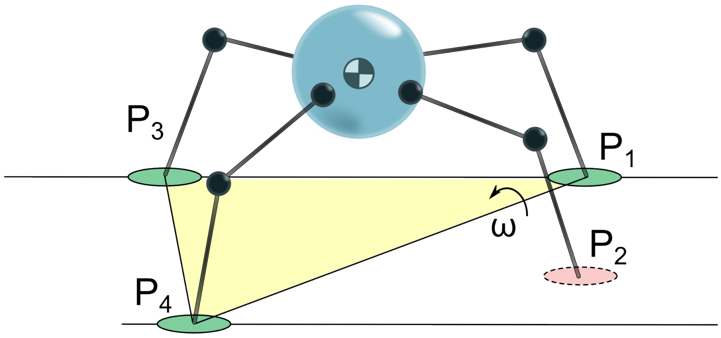

(c) Trotting gait after the application of disturbing energy, case of backward tilting.

Figure 3.4: Trotting gait and possible subsequent rotations in case of application of external disturbing energy.

ditions required to maintain a statically stable posture, and never consider the phenomena that happen when tumbling occurs.

As for the stability of dynamic walking, as far as the author is concerned, the discussion about it has not been done before, and dynamic walking was considered unstable from the beginning. Of course, there was a paper "Tumble Stability Margin and Safety Walk" [10], Iiyama and Yoneda expressed the idea of safety gait, which he defined as the walking motion which guarantees that vehicle maintains stability in every instance.

However, that paper did not include any methodology to actually quantify how much stability safety gait allows the robot to acquire. In comparison, my approach allows to fully quantify any influence that swinging legs have on stability of walking robot.

It has to be noted that static gait is a gait during which robot retains static stability, i.e. projection of its center of gravity lies within the boundaries of its supporting polygon. Specifically, this means that walking robot performing a static gait can cease motion in any moment of time, and remain stable, keeping the same posture. It then can continue motion as is nothing happened.

Dynamic gaits are different. Robot performing a dynamic gait cannot retain the posture, and will inevitably change it if locomotion is stopped or under any external disturbance.

Proposed method is applicable for both static and dynamic gaits, because it allows to account conveniently for the change of posture which happens in the aforementioned case (sudden stop of locomotion or external disturbance). It also accounts for vehicles velocity, which to a large extent influences robots stability during motion.

An idea about "stability" being an intrinsic property of dynamic walking may sound contradictory. From practical viewpoint, even if normal planned walking motion is disrupted, it is important to prevent complete tumbling and turn it into partial tumbling, because this may help to prevent robot's damage and to return to normal static or dynamic walking.

The gait that prevents complete tumbling and turns it into partial tumbling was specifically named a "Non-Tumbling Gait", or "NT Gait". Conditions that should be met in order to perform an NT Gait are discussed below.

Non-Tumbling Gait can be defined as a gait that prevents complete overturning of a robot, and maintains a standing posture even when a certain disturbing force is applied to robot's body from any direction.

Most important factor for an NT gait maintenance is the swinging leg motion. Conventional gait control olny accounts for a positional relation between standing legs and robot's CG, effectively neglecting an existence of the swinging legs. However, from an NT gait perspective, swinging legs massively influence the system. If a particular swinging leg moves too high above the ground, and/or too close to the supporting legs, it negatively influences the chances of maintaining stability.

Therefore, studying NT gait, the effect of the swinging legs must always be considered.

3.3 Generalized concept of the Directional Normalized Energy Stability Margin

In order to generate an NT gait resistant to large distirbing forces applied to robot's body from any direction, the first step was to introduce Directional Normalized Stability Margin, a new stability criterion that takes into account the dynamic effects of a tumbling motion, including the effect of the swinging leg when it forms a new ground foothold, as well as a directional disturbing force.

However, for the sake of simplification, derivation process that has been demonstrated above did not account for robot's body velocity, which was considered zero. Let us provide equations to calculate DNESM with velocity consideration.

Since robot body has a horizontal velocity $\mathbf{V}_b$, we are considering that rotational velocity $\mathbf{V}(\mathbf{V}(E_i), \mathbf{V}_b)_r$ is generated by both $\mathbf{V}(E_i)$ and $\mathbf{V}_b$.

P_i and P_j are neighbouring ground contact points. Edges of the supporting polygon and CG of the robot may be denoted as $\mathbf{P}_{i,j}$, and $G(x_G, y_G, z_G)$ correspondingly.

Main condition for overturning the robot is moving its CG from initial position G to a position $G_{(i,j)max}$ – an unstable equilibrium in rotation around $\mathbf{P}_{i,j}$ axis.

Thus, S_θ for the edge of the supporting polygon connecting ith and jth foothold may be easily computed through equation (3.1):

$$S_\theta = \frac{1}{2g}\Big(\frac{\sqrt{2gH_{i,j}}}{Z_{i,j}} - V_b\frac{B_{i,j\ body}}{B_{i,j}}\Big)^2. \tag{3.1}$$

Variables, necessary for computation of S_θ via (3.1), can be calculated through the following equations:

1. $H_{i,j}$, height difference between original CG position G and its highest possible position $G_{(i,j)max}$ above $\mathbf{P}_{i,j}$:

$$H_{i,j} = G_{(i,j)max\ z} - G_z, \tag{3.2}$$

where $G_{(i,j)max}$:

$$\mathbf{G}_{(i,j)max} = \frac{C_{i,j}}{\|\mathbf{P}_{i,j}\|}\hat{\mathbf{P}}_{i,j} + \cos\varphi_{max}\Big(\mathbf{P}_{iG} - \frac{C_{i,j}}{\|\mathbf{P}_{i,j}\|}\hat{\mathbf{P}}_{i,j}\Big) + \\ + \sin\varphi_{max}\frac{\mathbf{A}_{i,j}}{\|\mathbf{P}_{i,j}\|} + \mathbf{P_i}, \tag{3.3}$$

for which

$$\mathbf{A}_{i,j} = \begin{bmatrix} (y_j - y_i)(z_G - z_i) - (y_G - y_i)(z_j - z_i) \\ -(x_j - x_i)(z_G - z_i) + (x_G - x_i)(z_j - z_i) \\ (x_j - x_i)(y_G - y_i) - (x_G - x_i)(y_j - y_i) \end{bmatrix}, \tag{3.4}$$

and

$$C_{i,j} = (x_G - x_i)(x_j - x_i) + (y_G - y_i)(y_j - y_i) + \\ + (z_G - z_i)(z_j - z_i). \tag{3.5}$$

Also, a maximum angular displacement of robot's CG $\varphi_{\substack{max \\ i,j}}$ can be found as:

$$\varphi_{\substack{max \\ i,j}} = \arctan(D_{ij}), \tag{3.6}$$

where

$$D_{i,j} = \frac{(x_j - x_i)(y_G - y_i) - (x_G - x_i)(y_j - y_i)}{\|\mathbf{P}_{i,j}\|(z_G - z_i) - \frac{C_{i,j}}{\|\mathbf{P}_{i,j}\|}(z_j - z_i)}. \tag{3.7}$$

2. Coefficient $Z_{i,j}$ for a $\mathbf{P}_{i,j}$ axis:

$$Z_{i.j}^2 = \Big(\frac{B_{i,j}}{\|\mathbf{P}_{i,j} \times \mathbf{P}_{iG}\|^2}\Big)^2 \mathbf{A}_{i,j}^T \mathbf{A}_{i,j}, \tag{3.8}$$

for which coefficient $B_{i,j}$:

$$B_{i,j} = \Big[\big((y_j - y_i)(z_G - z_i) - (y_G - y_i)(z_j - z_i)\big)\cos\theta + \\ + \big(-(x_j - x_i)(z_G - z_i) + (x_G - x_i)(y_j - y_i)\big)\sin\theta\Big]. \tag{3.9}$$

3. Similarly, coefficient $B_{i,j\ body}$:

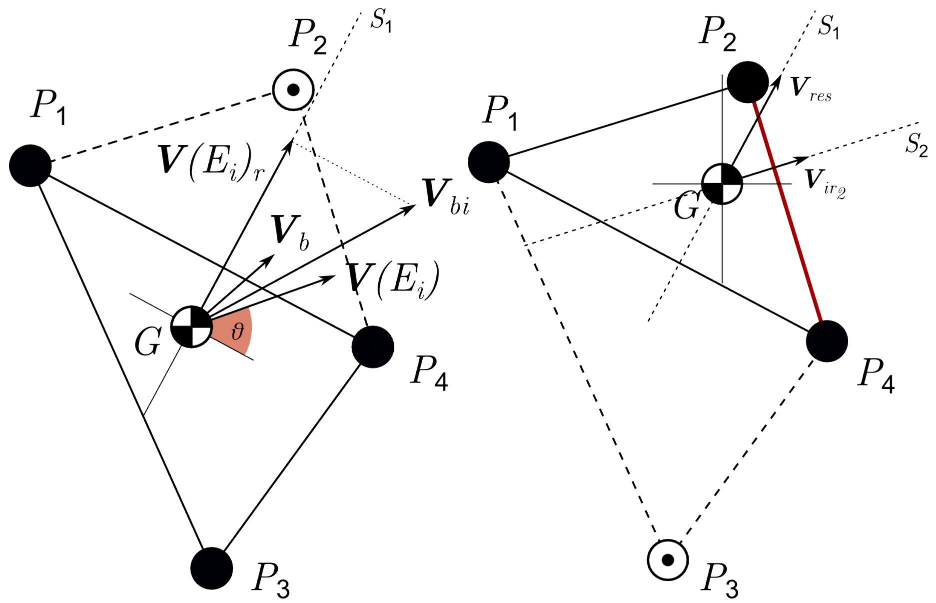

(a) First rotation.

(b) Second rotation, variant with tumbling around P_2P_4 line.

Figure 3.5: Sequence of destabilized motion (partial tumbling) after the application of disturbing input energy E_i.

$$B_{i,j\ body} = \Big[\big((y_j - y_i)(z_G - z_i) - (y_G - y_i)(z_j - z_i) \big) \cos\gamma + \\ + \big(-(x_j - x_i)(z_G - z_i) + (x_G - x_i)(y_j - y_i) \big) \sin\gamma \Big], \tag{3.10}$$

where γ is the direction angle of robot's body velocity $\mathbf{V}_b$.

3.3.1 Expansion of S_θ for the generalized case of partial tumbling

As it was explained above, in presence of the swinging leg, when disturbing force is high enough to cause robot's rotation around a given edge of the supporting polygon, the leg may block robot's motion. In order to explain this tumbling sequence in detail, let us refer to Fig. 3.3. There are two possible stages of rotation, and we will refer to them as "first rotation" and "second rotation".

We will be using the case of a crawling gait pictured on Fig. 3.3 as an illustration to our explanation and subsequent calculations.

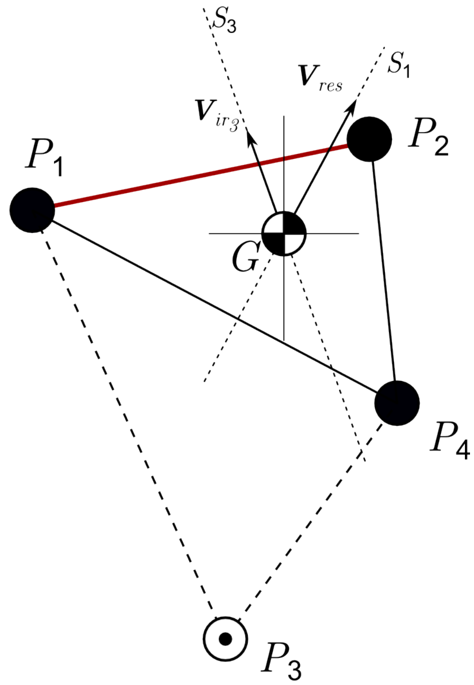

Figure 3.6: Second rotation, variant with tumbling around P_1P_2 line.

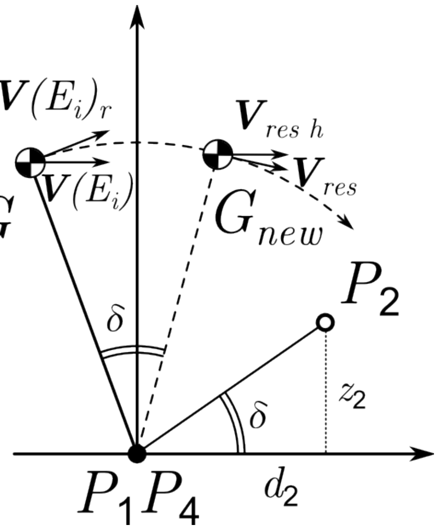

Figure 3.7: Side view of the first rotation.

In case of Fig. 3.3, first rotation is a rotation of robot's CG around P_1P_4 edge of the supporting polygon $P_1P_3P_4$ (top view diagram shown on Fig. 3.5a). If input energy E_i is sufficient, and so is input velocity $\mathbf{V}(E_i)$, it may force the robot to overturn around P_1P_4. If that is the case, leg P_3 loses its contact with the ground, while leg P_2, on contrary, gains it. This motion results in a change of the supporting polygon from $P_1P_3P_4$ to $P_1P_4P_2$ (Fig. 3.3b, 3.5b).

If initial disturbing energy E_i is high enough, robot's movement can continue in a second rotation phase either around P_2P_4 (in S_2 plane, Fig. 3.5b), or around P_1P_2 (in S_3 plane, Fig. 3.6), depending on the position of the swinging leg P_2 and direction of motion of the CG.

For the purpose of illustration, let us suppose that second rotation occurs around P_2P_4, as on Fig. 3.5b. Let us discuss the process of calculation of S_θ in such case in detail.

Calculation of S_θ for the first rotation

For the first rotation, we will not be calculating a typical S_θ as the one we discussed before. This is because previously we were suggesting that disturbance input energy E_i should be sufficient to rotate CG around P_1P_4 edge on angle φ_{max}. But in case of partial tumbling, the motion of robot's CG is constrained by existing swing leg (e.g. P_2). Thus, it needs to be moved on angle δ, or the angular distance which swing leg P_2 should travel before hitting the ground (Fig. 3.7).

In such case, we can substitute angle θ_{max} with angle δ. Therefore, we must first calculate angle δ based on the coordinates of swing leg P_2 before its collision with the ground. It can be expressed as:

$$\delta = \arctan\left(\frac{z_2}{d_2}\right), \tag{3.11}$$

where z_2 is the height of the swing leg P_2, d_2 is the distance between projection of P_2 on a horizontal plane and P_1P_4 edge of the supporting polygon.

In turn, distance d_2 can be easily calculated as

$$d_2 = \frac{(y_1 - y_4)x_2 + (x_4 - x_1)y_2 + (x_1y_4 - x_4y_1)}{\sqrt{(y_1 - y_4)^2 + (x_4 - x_1)^2}}. \tag{3.12}$$

New position of robot's CG in rotation around P_1P_4 edge can be calculated from equation (3.3) by substituting φ_{max} with δ which can be found through equations (3.11) and (3.12):

$$\mathbf{G}_{first} = \frac{C_{1,4}}{\|\mathbf{P}_{1,4}\|}\hat{\mathbf{P}}_{1,4} + \cos\delta\Big(\mathbf{P}_{1G} - \frac{C_{1,4}}{\|\mathbf{P}_{1,4}\|}\hat{\mathbf{P}}_{1,4}\Big) + \\ + \sin\delta\frac{\mathbf{A}_{1,4}}{\|\mathbf{P}_{1,2}\|} + \mathbf{P_1}. \tag{3.13}$$

Knowing G_{first}, the new position of CG, we can calculate the height difference $H_{1,4}$ between it and initial position G:

$$H_{1,4} = G_{first\ z} - G_z. \tag{3.14}$$

Also, from equation (3.9) we can define coefficient $B_{1,4}$, and, from (3.8), we can calculate $Z_{1,4}$. Subsequently, from equation (3.1) it is easy to find $S_{\theta\ first}$ for P_1P_4 edge of the supporting polygon:

$$S_{\theta\ first} = \frac{1}{2g}\Big(\frac{\sqrt{2gH_{1,4}}}{Z_{1,4}} - V_b\frac{B_{1,4\ body}}{B_{1,4}}\Big)^2. \tag{3.15}$$

Calculation of $\mathbf{S}_\theta$ for the second rotation

It is important to highlight that after the first rotation robot's body acquires a residual velocity $\mathbf{V}_{res}$ (Fig. 3.5b, 3.7). Projection of this residual velocity on a horizontal plane represents a body velocity $\mathbf{V}_{b\ second}$, which is an initial condition for the second rotation.

Another important point is that we cannot vary angle θ_{second} (direction of the input velocity $\mathbf{V}_{second}(E_i)$) during the second rotation. This is because robot's motion in this stage is not independent, but is only a continuation of the motion initiated at the stage of first rotation under the influence of previously applied disturbance energy E_i. Thus, the directions of $\mathbf{V}_{res\ h}$, horizontal projection of residual velocity, and input velocity for the second rotation $\mathbf{V}_{second}(E_i)$ coincide. Therefore, physical meaning of S_θ for the second rotation is how much energy is required to overturn the robot around the edge of the supporting polygon *in addition* to existing residual energy from the first rotation (represented in the form of residual velocity $\mathbf{V}_{res}$).

In such case, $S_{\theta\ second}$ can be calculated through equation (3.1), with a consideration that $\theta_{second} = \gamma_{second}$, and $V_b = V_{res\ h}$. Thus, $B_{2,4} = B_{2,4\ body}$, and equation for its calculation will look like

$$B_{2,4} = \Big[\big((y_4 - y_2)(z_G - z_2) - (y_G - y_2)(z_4 - z_2)\big)\cos\theta_{second} + \\ + \big(-(x_4 - x_2)(z_G - z_2) + (x_G - x_2)(y_4 - y_2)\big)\sin\theta_{second}\Big]. \tag{3.16}$$

Height difference $H_{2,4}$ must be calculated in regard to G_{first}, position of CG after the first rotation:

$$H_{2,4} = G_{2,4\ z} - G_{first\ z}. \tag{3.17}$$

Finally, equation (3.1) for calculation of $S_{\theta\ second}$ can be written as

$$S_{\theta\ second} = \frac{1}{2g}\Big(\frac{\sqrt{2gH_{2,4}}}{Z_{2,4}} - V_{res\ h}\Big)^2. \tag{3.18}$$

After all those calculations, computed S_θ for both rotations, expressed in equations (3.15) and (3.18), can be combined, thus giving an understanding of total Dynamic Normalized Energy Stability Margin for a given posture in presence of the swinging leg:

$$S_{\theta\ total} = S_{\theta_{first}} + S_{\theta_{second}}, \tag{3.19}$$

where $S_{\theta\ first}$ represents an energy required to perform first rotation, and $S_{\theta\ second}$ represents an additional energy required for robot to continue tumbling motion.

Chapter 4

Validation of Generalized DNESM for Non-Tumbling Gait

4.1 Modified tumbling experiment and simulation for a simple model

As in the previous chapter on Directional Normalized Energy Stability Margin, calculation of S_θ was validated by performing a numerical simulation, and then conducting a tumbling experiment with a simple model of a robot, measuring S_θ manually, and comparing our results with a simulation for the same model.

In order to perform a validation of S_θ with swinging leg consideration, experiment with a similar, but slightly modified setup was conducted.

Tumbling experiment setup shown on Fig. 4.1a was essentially the same as in previous experiment. However, for the purpose S_θ validation, body 4 had an additional "swinging" leg – a shorter leg elevated 5 mm above the surface. After the application of impact force and subsequent first rotation around an edge of the existing supporting polygon, swinging leg prevented overturning and helped to create a secondary supporting polygon (partial tumbling).

Experimental process was done to measure the lowest height of the pendulum that defined a corresponding potential energy required to overturn the body around the edge of a secondary supporting polygon. After several iterations for each angular position, it was possible to make a measurment of S_θ with a certain precision.

Results of the experiment were then compared to the results of numerical

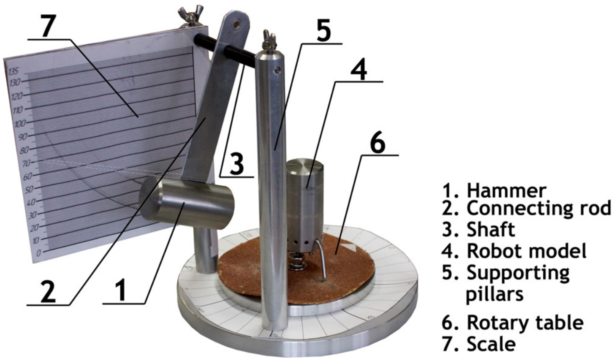

(a) Impact table.

(b) Robot body model 4 (swing leg height is 5 mm), before first rotation.

(c) Robot body model after first rotation.

Figure 4.1: Modified experimental setup.

simulation for the tumbling model, and are shown on Fig. 4.2.

4.2 Simulation for a model of a walking robot

Currently, there is a new walking robot in development at Fukushima Laboratory, called TITAN-XIII (Fig. 4.3). This is a lightweight machine built specifically for research on gait control and stability of multi-legged locomotion. Although work on the robot is not yet completed, it was decided to apply the theory of S_θ and examine stability of TITAN-XIII beforehand.

To do so, a numerical simulation based on the geometry of TITAN-XIII performing a trotting gait was developed. The simulation allowed to calculate S_θ in all stages of motion for all edges of all possible supporting polygons. Main purpose of such simulation was to measure the minimum of S_θ throughout the motion sequence, and suggest ways to improve locomotion stability, thus creat-

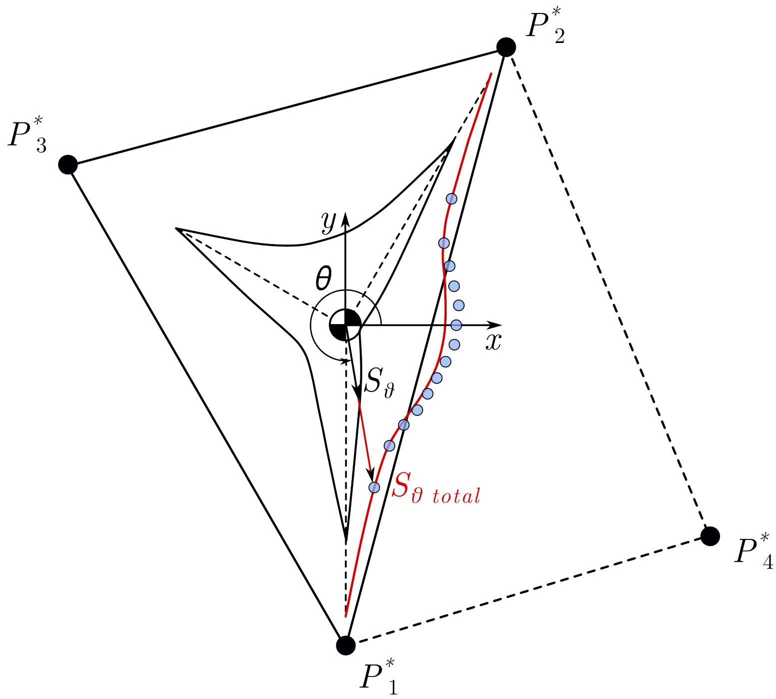

Figure 4.2: Experimental results (shown as dots) and derived S_θ accounting for existence of the swinging leg (shown as a red line). DNESM S_θ for $P_1P_2P_3$ supporting polygon without swinging leg consideration is presented for comparison (shown in black).

Figure 4.3: TITAN-XIII walking robot.

ing a Non-Tumbling gait for a particular robot.

It has to be highlighted, that the goal of this simulation was not to experiment on the gait generation, but to study the parameters of motion that influence stability of the robot, as well as to find the best posture for one particular gait. In other words, its goal was to analyze the gait in terms of stability and define ways to improve it, not to create an entirely new gait with a different planar trajectory of the swing leg.

Subsections below discuss the specifics of the simulation and its results.

4.2.1 Simulation assumptions

Similarly to previous simulations, walking simulation was done with the following assumptions:

- External energy E_i is supplied to the system in a horizontal plane, and, thus, $\mathbf{V}(E_i)$ lays in the horizontal plane as well.
- Friction in the footholds is infinite, and slipping does not occur.
- Legs are massless, and robot's mass is concentrated in the body.
- Angular velocity of the body $\omega_{\mathbf{b}} = 0$.
- Simulation is conducted with an assumption that the surface is flat.
- In simulated trotting gait, change of the supporting pair of legs happens instanteneously.

4.2.2 Parameters of robot's motion

The equations used to control CG position and its velocity are as follows.

Position of CG is calculated as:

$$G_x(t) = Ae^{st} + Be^{-st}, \tag{4.1}$$

where $A = (V_0/s + x_0)/2$, $B = (-V_0/s + x_0)/2$, $s = \sqrt{g/G_z(t)}$.

CG velocity is calculated as

$$V_b(t) = s(Ae^{st} - Be^{st}), \tag{4.2}$$

and minimum initial velocity $V_0 = -G_{x0}\sqrt{g/G_{z0}}$.

As it is clear from equation (4.2) and Fig. 4.5 robot's body velocity is highest in the the beginning of each step. As the motions progresses, it decreases and, at the point when robot's CG is located above the supporting line, robot's body velocity reaches its minimum. After this, it enters a phase of acceleration, and reaches minimum initial velocity V_0 towards the end of the current step and the beginning of the next step.

Such sophisticated velocity control, despite intorucing rapid acceleration and deceleration, allows to achieve greater speed and grater stability of the posture. Specifics of this approach are discussed in [19].

In the context of validation of S_θ, consideration of robot's body velocity $\mathbf{V}_b$ brings the simulation closer to real life, and allows to make better judgements about the applicability of S_θ.

We have conducted several types of simulation where robot was performing a step of a trot gait. Simulation types are as follows:

- Varying swing leg height.
- Varying CG height.
- Varying velocity simulations.

4.2.3 Posture stability map

Performed simulation was based on a trot gait with a fixed stride (150 mm). During the simulation, the minimum S_θ was computed throughout the motion sequence. By varying the wideness of the posture, it was possible to obtain different minimum measurements of S_θ. Each simulation was conducted in 30 different configuration positions across the service area for that particular stride (service area for 150 mm stride is shown in dark grey on Fig. 4.4, and M is the middle point of the stride).

Position of a stride's middle point M defined the posture.

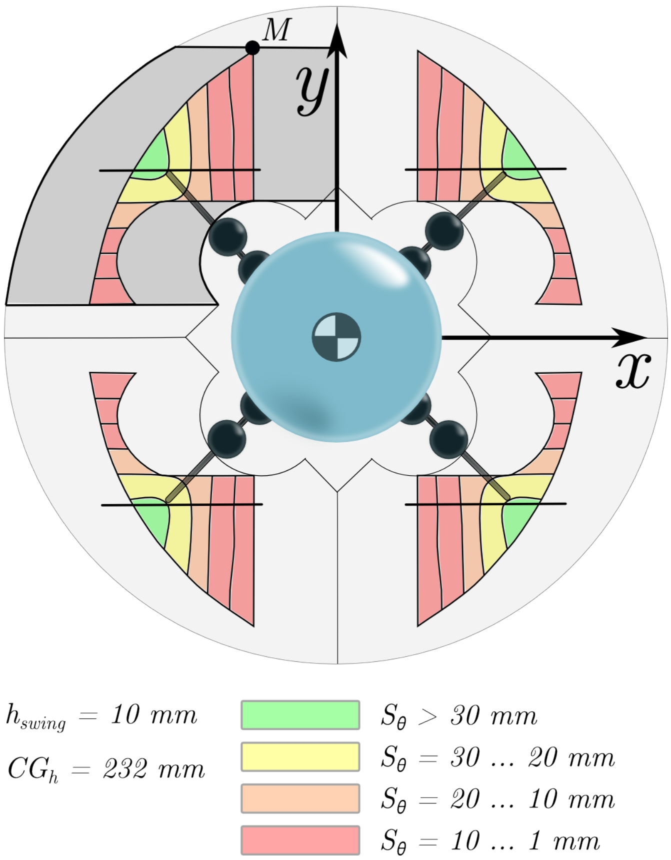

Figure 4.4: Areas of minimum S_θ for TITAN-XIII walking robot performing a trotting gait with a fixed stride. The best $S_\theta = 0.055m$.

Such simulation allowed to generate a stability map, a simple representation of safe and unsafe postures and footholds (Fig. 4.4). Light green areas represent zones with most stable postures, while pinkish areas show most unstable postures.

4.2.4 Direction of minimum S_θ during motion

Firstly, basic behavior of S_θ was studied, such as the changes in direction of minimum S_θ during a step of our model of TITAN-XIII. Although walking cycle consists of two steps performed by interchanging pairs of legs, due to symmetrical nature of the examined walk it is enough to consider only one step.

Changes of S_θ throughout one step of a simulated TITAN-XIII walking robot

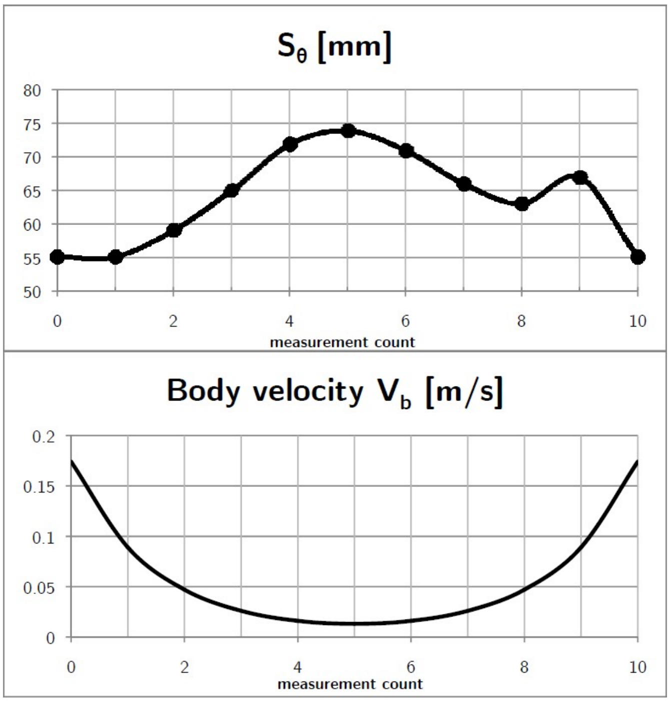

Figure 4.5: Behavior of S_θ througout the step of TITAN-XIII walking robot.

performing trot gait are presented on Fig. 4.5, and actual contour of S_θ for each measurement can be seen on Fig. 4.6.

It is interesting to notice that, during the motion, direction of minimum S_θ changes (Fig. 4.6). From Fig. 4.5 it is clear that this happens because of the changes of robot's velocity (Fig. 4.5). Additionally, the way S_θ changes throughout the step is not trivial. In points 0 to 2, stability is low, as the velocity is high and directed forward. As the decrease of body velocity $\mathbf{V}_b$ becomes significant, stability increases (points 3 to 5), achieving its maximum in point 5, where velocity is minimum, and posture is effectively a square. S_θ starts decreasing in point 6 and achievs a local minimum in point 8, but because a pair of swinging legs is moved forward and velocity is not yet high enough, the minimum stability is directed backwards.

A sudden increase of stability in point 9 is of particular interest. It occurs because of the increase of velocity (directed forward) that counteracts the neg-

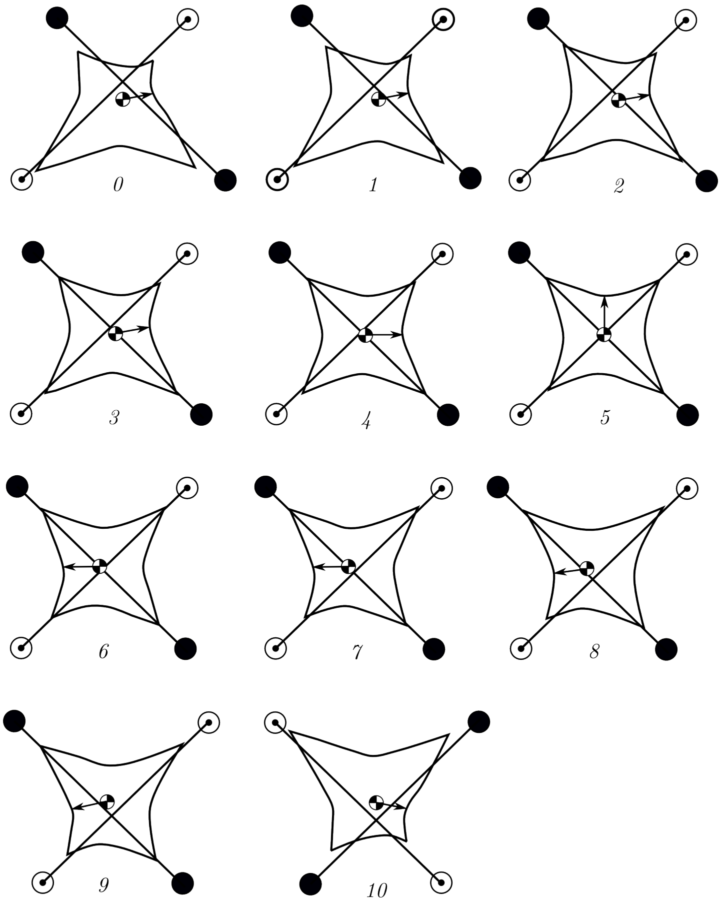

Figure 4.6: Countour of S_θ throughout the step of TITAN-XIII walking robot.

ative effect of the swinging pair of legs which affect S_θ and decrease it in the backward direction.

Finally, at point 10, when the step is finished and another pair of legs becomes supporting, S_θ equals to measurement in point 0, and contours in 0 and 10 are symmetrical.

It is important to highlight, that this simple analysis shows that Directional Normalized Energy Stability Margin (or S_θ) can be used to estimate stability of multi-legged robot in *every* moment throughout the motion. Not only it provides the insights about which phase of the step is most stable and unstable, but also shows interesting effects that posture and velocity control may have on stability during walking.

4.2.5 Varying height of the swing leg

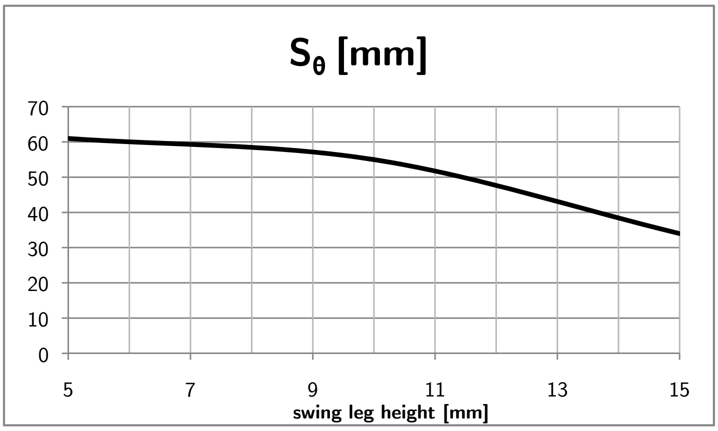

Figure 4.7: Behavior of S_θ in case of increasing swing leg height.

In order to gain more insights about how different parameters of robot's posture influence S_θ, a simulation with varying swing leg height was performed: 5, 10, and 15 mm above the ground for each series of the simulation. Position of robot's CG remained at 232 mm above the ground.

Dependency between S_θ and height of the swing leg is shown on Fig. 4.7. It is clear that increase of swing leg height results in decrease of multi-legged locomotion stability, as indicated by S_θ.

4.2.6 Varying height of robot's CG

Previous simulations were conducted with a consideration that robot's center of gravity has a constant height of 232 mm above the surface (default height of the CG of TITAN-XIII). In order to understand how the decrease of CG height influences locomotion stability, a set of experiments, where CG height was gradually decreased to 200 mm, was done.

As one can see from results of the simulation presented on Fig. 4.8, decrease of robot's CG height allows to achieve a significant increase in locomotion safety. By lowering CG it was possible to increase minimum S_θ to 73 mm. Thus, 16% decrease in CG height resulted in 33% increase in S_θ.

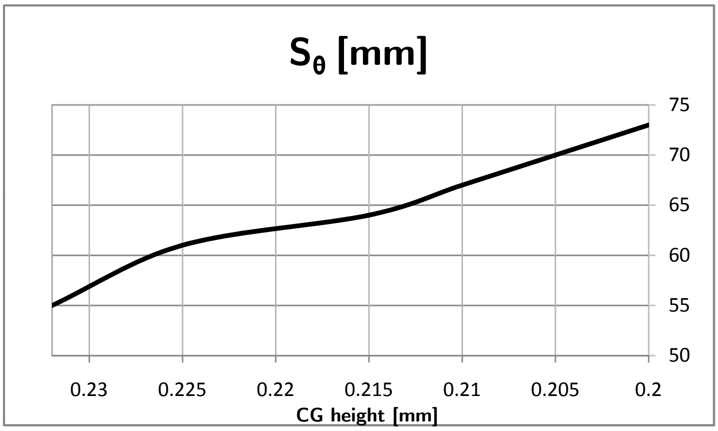

Figure 4.8: Behavior of S_θ in case of decreasing CG height.

4.2.7 Varying constant velocity

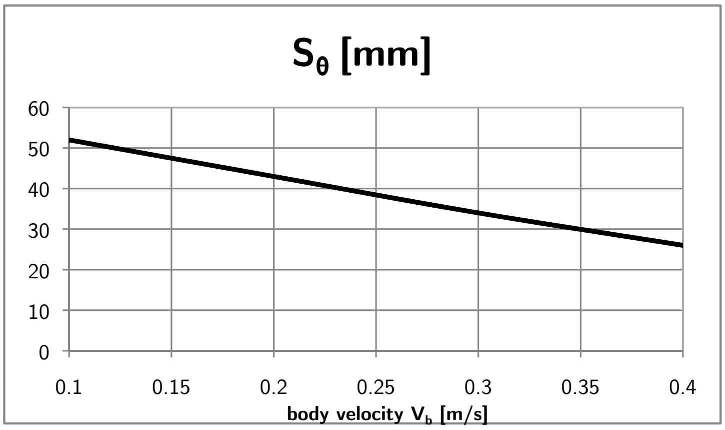

Figure 4.9: Linear decline of S_θ caused by the increase of robot's body velocity.

Finally, in order to understand the effect which body velocity has on safety margin, a series of simulations where robot's velocity was constant throughout the motion sequence was performed. Velocity was incrementally increased in each modeling session. Four velocities considered were: 0.1 m/s, 0.2 m/s, 0.3 m/s, and 0.4 m/s (maximum possible velocity for TITAN-XIII walking robot is 0.7 m/s).

It is obvious that increase in the velocity would result in a decline of stability.

Results of the simulation are shown on Fig. 4.9. As one can see from the plot, the decrease of stability caused by increase in velocity is essentialy linear.

4.3 Tumbling experiment with Titan-XIII and the effect of the swinging leg height

Apart from the simulation whose goal was to generate a posture stability map, it was required to conduct a more realistic experiment with a real-life robot.

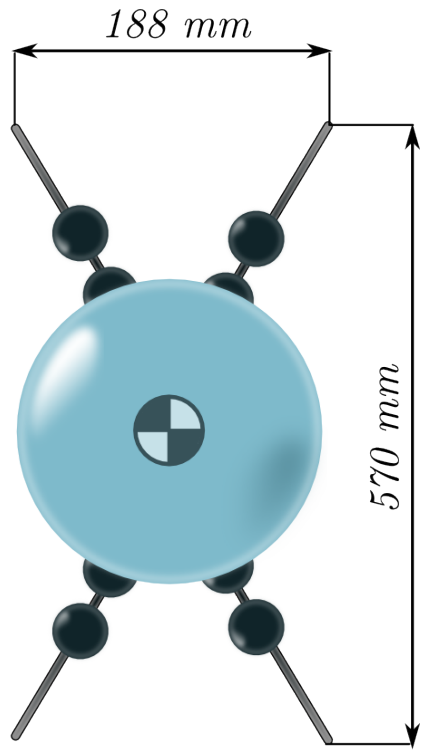

Figure 4.10: Posture of Titan-XIII robot used for the swing leg height experiment.

Experiment was based on the following scenario. Titan-XIII walking robot was performing a trot gait with a 100 mm stride on a flat surface with a relatively narrow posture (Fig. 4.10). There were two possible ways to tumble the robot during motion: (1) to apply an external force to destabilize the robot, (2) to suddenly stop the robot during motion, thus causing it to tumble under the influence of it's own inertial factors. Because applying an external force would mean hitting robots body during motion, this option was not viable. Instead, it was decided to resort to stopping the robot.

A step of Titan-XIII was divided into phases, where 0.0 was considered as the beginning of the step, and 0.5 as the end of the step.

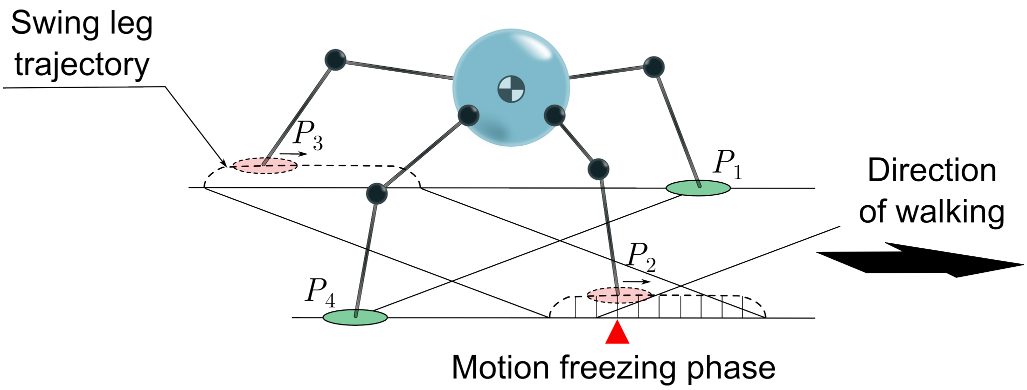

Figure 4.11: Scheme of Titan-XIII performing a trot gate with a freezing phase marked with red triangle.

An arbitrary phase of motion (0.15) was chosen for the moment of a sudden stop (Fig. 4.11). Robot's velocity at that point was measured, and DNESM S_θ at that point was calculated for two cases of the swing leg height: 50 mm and 15 mm.

The energy from robot's velocity was then compared to energy required to cross DNESM. It turned out that, according to the simulation, robot would appear stable in case of 15 mm swing leg height ($S_\theta = 6.453 \times 10^{-3}$, stability decrease from robot's body velocity: 1.215×10^{-3}), and would tumble in case of 50 mm height ($S_\theta = 2.045 \times 10^{-4}$, stability decrease: 1.215×10^{-3}).

Indeed, an experiment with Titan-XIII proved that the results of the simulation, and, hence, the idea beyond DNESM, were valid.

Additionally, a tumbling threshold of a swing leg height was defined. Theoretical result suggested that at 0.15 step phase, robot would tumble if a swing leg height was more than 37 mm. Practical experiment showed that, in this case, actual threshold swing leg height is 30 mm.

Such result is the consequence of one or a combination of intrinsic effects: compliance, slipping, and large error in the control system of the robot.

4.4 S_θ as a source of insigths about design of multi-legged robots

(a) Bug as one of the most vivid examples of insect type posture (wide, CG height is low).

(b) Horse as an example of mammal type posture (narrow/elongated, CG is elevated).

Figure 4.12: Examples of insect and mammal postures in animals.

TITAN-XIII walking robot, shown on Fig. 4.3, was specifically designed for experiments in gait control and locomotion stability of multi-legged vehicles. Before building the robot, it was implicitly agreed that from design standpoint it would be better to pursue an insect type construction, instead of a more widespread mammal type. Insect type (Fig. 4.12a) means a robot design which allows wide postures with an ability to position center of gravity at a low height. Mammal type design is, on contrary, presupposes a narrow posture (Fig. 4.12b) and a high position of the CG.

Insect type design of TITAN-XIII was justified by the fact that insects, due to their wide postures, have greater stability than mammals. However, such proposition lacked scientific backing. So far, there has been no significant research aimed on quantitative estimation of the advantage which insect type design has over mammal type in terms of stability.

Now, Directional Normalized Energy Stability Margin gives us an insight into how significantly different those two types of design/postures are in terms of stability.

Table 4.1: Studied mammal- and insect-type postures for Titan-XIII.

Posture	CG height	Stride ratio	Stability margin
Mammal	232 mm	0.46	11 mm
Insect	200 mm	0.97	73 mm

Stability of insect and mammal postures presented on Fig. 4.13 and Table 4.1 was compared. Apart from one being wider than the other, insect type posture featured a CG height of 200 mm, while mammal type posture had 232 mm height, which is not the highest TITAN-XIII is capable of, but, nevertheless, suitable for illustration.

As a result, minimum stability margin for insect posture was 73 mm, and minimum stability margin for mammal posture was only 11 mm, which constitutes only $15,1\%$ of the stability of an insect type posture for Titan-XIII.

Stability map provided on Fig. 4.4 may serve as an additional illustration of the fact that not only more narrow postures have reduced stability as known before, but that in case of narrow mammal type postures, stability is reduced radically.

It is important to notice that discussion of mammal stability versus insect stability should be done in the context of complexity of the control system of a robot in question. Insect-type posture allows to use more simple motion control and may save researcher a lot of time when the focus of his or her research is not related to stability or balancing.

Mammal-type posture, on contrary, may require a sophisticated control and

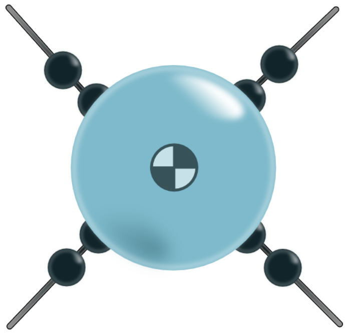

(a) Insect type posture

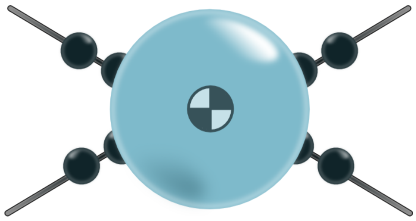

(b) Mammal type posture

Figure 4.13: Studied insect- and mammal-type postures for Titan-XIII.

can be an interesting domain to explore for scientists who perform research in complex motion control.

Therefore, when designing a new walking robot, researchers must consider possible range of its applications, as well as types of terrain on which a machine in question will operate. They must also define stability requirements for such robot. Based on this knowledge, it is possible to find the most suitable design of a robot: insect or mammal.

Consequently, such consideration will allow them to better estimate the complexity of a control system required to make the robot operational. Thus, thinking about stability is important even *before* the start of the design work.

Chapter 5

Conclusions and Future Work

5.1 Conclusions

This thesis discussed the problems that prevent widespread diffusion of multi-legged robots technology. While being an exciting and inspiring research subject, legged robots are still exotic and are usually used for research purposes, instead of practical field application.

Particular focus of this thesis was the issue of stability and robustness of multi-legged locomotion in various settings: flat ground, slope, etc. Before diving into the subject of stability, this work gave a brief outline of the history of walking robots, as well as the history of previous research on their stability. To narrow down the topic to an easily digestible piece, this thesis discusses mainly quadrupedal robots. However, the findings of this research can be applied to any type of walking robots with a number of legs more than two.

Discussion about multi-legged stability started with an idea that conventional stability margins do not account for the direction of an external disturbing influence (an input energy E_i). It was suggested that such simplification can actually greately limit the understanding and precision of quantification of stability of legged robots.

Such suggestion led to a proposition of Directional Normalized Energy Stability Margin (or S_θ), a stability measurement which, unlike previous criteria, accounts for the direction of an input energy E_i.

Another interesting idea that was discussed is a so-called Non-Tumbling Gait. Non-Tubling Gait was born out of consideration that before now, discussion about swinging legs was virtually excluded from the discourse of multi-legged stability. However, existense of swinging leg not only may increase the stability and reliability of multi-legged locomotion, but also make walking robots intrinsically stable, if their motion control performed right.

Non-Tumbling Gait relies on the notion of Directional Normalized Stability Margin, since it is important to know both maximally and minimally stabile directions during robots motion.

Directional Normalized Energy Stability Margin was validated by simulation and tumbling experiment; both were done with and without consideration about the existence of swing leg. Simulation was performed for an actual walking robot, Titan-XIII.

Finally, a tumbling experiment with Titan-XIII was performed, and results of the experiment corresponded with results of the simulation. However, it was found out that certain effects like compliance or slipping may influence the stability as well.

Research that served as a foundation of this thesis has been published in two papers ([22] and [23]). First paper focuses on proposition and derivation of Directional Normalized Energy Stability margin, and also on its validation for the case of flat ground and slope. The idea of Non-Tumbling Gait is briefly outlined, but no discussion is done. Second paper focuses on thorough discussion about Non-Tumbling Gait, generalized concept of DNESM, which is augmented to consider the case of a two-phase rotation occurring in the presence of the swinging leg. Additionally, this paper discusses a simulation done for a quadruped robot performing a trot gait.

Speaking of how this work contributes to development of walking robots, from the standpoint of control, this research enables researchers to better quantify stability of their robots and create more efficient control algorithms for rough-terrain locomotion. For example, currently, there are a lot of researches (e.g., [24], [25]), in which authors study performance of a walking robots on an uneven surface, but keep using Static Stability Margin, which is highly inaccurate, and is only applicable to the case of a flat ground. Using DNESM, which accounts for the position of all legs, both standing and swinging, such research can be greatly improved.

Additionally, this thesis discussed profound implications which thinking about stability of multi-legged robots can bear on their design. Currently, a lot of researchers build robots first, and then study their behavior after. This work argues that we can (and should) estimate required stability of a robot before starting the design process, because it may lead to better decisions about functional requirements of a multi-legged machine in question.

5.2 Future Work

This thesis was heavily focused on the fundamental theory of multi-legged stability. Even if it is verified and validated, almost every theory requires practical application before it makes lives of researchers easier. Theory of Directional Normalized Energy Stability margin and Non-Tumbling Gait must be applied to different types of multi-legged robots.

But it must be highlighted that since DNESM and NT Gait depend on quite a few parameters (robot's velocity, swing leg trajectory, etc.), their generation is data intensive. That data must be gathered properly, and that requires installing measurement devices on the machines.

Additionally, the effect of dynamic parameters should be studied (the effect of compliance and torques in the joints, ground compliance, bouncing, etc.). Tumbling experiment with Titan-XIII robot demonstrated that such parameters may have certain influence on the value of Directional Normalized Energy Stability Margin.

Currently, newest walking robots, such as Titan-XIII and Titan-XII, created in Fukushima Lab, do not have certain on-board sensors, and that significantly limits opportunities for complex control which might be required to fully utilize DNESM and NT Gait. Thus, researchers working on those robots must consider installing sensors that can provide them with solid numerical data about all parameters of robot's motion in real time.

Speaking of robot control, it would be interesting to employ various methods of adjustment of robot's posture according the DNESM and NT Gait theory. Such methods may vary from precise optimal control to maximize stability margin, or more natural (or higher-level) fuzzy logic or neural networks control principles.

References

[1] P. Gonzalez de Santos, E. Garcia, J. Estemera,“Quadrupedal Locomotion. An Introduction to the Coltrol of Four-legged Robots”, Springer, 2006.

[2] M. F. Silva, J. A. Tenreiro Machado, “A Historical Perspective of Legged Robots”, *Journal of Vibration and Control*, vol. 13, n0. 9-10, pp. 1447-1486, 2007.

[3] Springer Handbook of Robotics, ed. B. Siciliano, O, Khatib, *Springer*, pp. 361-398, 2008.

[4] M. Raibert, “Legged Robots”, *Communications of the ACM*, vol. 29, no. 6, pp. 499-514, 1986.

[5] H. C. Wong and D. E. Orin, “Dynamic Control of a Quadruped Standing Jump”, in *Proceedings of IEEE International Conference on Robotics and Automation*, vol. 3, pp. 346-351, 1993.

[6] H. C. Wong, D. E. Orin, “Control of a Quadruped Standing Jump over Irregular Terrain Obstacles”, *Autonomous Robots*, vol. 1, pp. 111-129, 1995.

[7] R.B. McGhee and A.A. Frank, “On the Stability Properties of Quadruped Creeping Gaits” *Mathematical Biosciences*, vol. 3, pp. 331-351, 1968.

[8] D. A. Messuri and C.A. Klein, “Automatic Body Regulation for Maintaining Stability of a Legged Vehicle During Rough-Terrain Locomotion”, *IEEE Journal of Robotics and Automation*, vol. RA-1(3), 1985, pp. 132-141.

[9] S. Hirose, H. Tsukagoshi, K. Yoneda, “Normalized Energy Stability Margin: Generalized Stability Criterion for walking vehicles”, *Proceedings of*

International Conference on Climbing and Walking Robot, Brussels, Belgium, pp. 71-76, 1998.

[10] S. Hirose, K. Yoneda, H. Iiyama, “Tumble Stability Margin and Safety Walk”, *Annual Conference of Japanese Society for Robotics and Mechatronics*, no. 930-40, pp. 310-313, 1993.

[11] K. Yoneda, S. Hirose, “Dynamic and Static Gait of a Quadruped Walking Vehicle on a Winding Path”, *Advanced Robotics*, vol. 9, no. 2, pp. 125-136, 1995.

[12] K. Yoneda, H. Iiyama, and S. Hirose, “Intermittent Trot Gait of a Quadruped Walking Machine. Dynamic Stability Control of an Omnidirectional Walk”, *Proceedings of the 1996 IEEE lntemational Conference on Robotics and Automation*, pp. 3002-3007, 1996.

[13] S. Hirose, K. Yoneda, R. Furuya, T. Takagi, “Dynamic and Static Fusion Control of Quadruped Walking Vehicle”, *Proceedings of IEEE/RSJ International Workshop on Intelligent Robots and Systems*, pp. 199-204, 1989.

[14] K. Arikawa, S Hirose, “Development of quadruped walking robot TITAN-VIII”, *Intelligent Robots and Systems ’96, IROS 96, Proceedings of the 1996 IEEE/RSJ International Conference on*, vol.1, no. 4-8, pp. 208-214, 1996.

[15] S. Hirose, H. Tsukagoshi, K Arikawa, “Development of Quadruped Walking Robots TITAN-VII and TITAN VIII, Final Report”, *Research Program on Mechanism for Emergent Machine Intelligence*, pp. 535-545, 1999.

[16] F. Gantmacher,“Lectures in Analytical Mechanics”, MIR Publications, 1975.

[17] K. Yoneda and S. Hirose, “Tumble Stability Criterion of Integrated Locomotion and Manipulation”, *Proceedings of International Conference on Intelligent Robots and Systems*, pp. 870-876, 1996.

[18] K. Yoneda and S. Hirose, "Three-Dimensional Stability Criterion of Integrated Locomotion and Manipulation", *Journal of Robotics and Mechatronics*, vol. 9, no. 4, pp. 267-274, 1997.

[19] S. Kitano, G. Endo, S. Hirose, "Development of Light Weight Quadruped Robot TITAN XIII", *The Robotics and Mechatronics Conference 2013*

[20] http://www-robotics.jpl.nasa.gov/systems/system.cfm?System=11

[21] http://cyberneticzoo.com/

[22] S. Hirose, E. Lazarenko, G. Endo, "Non-Tumbling Gait and Directional Normalized Energy Stability Margin", *Advanced Robotics*, 2013 (in press).

[23] E. Lazarenko, S. Kitano, S. Hirose, G. Engo, "Non-Tumbling Gait for Multi-Legged Robots and its Directional Normalized Energy Stability Margin", *ISRN Robotics*, 2013 (in press).

[24] J. Z. Kolter, M. P. Podgers, A. Y. Ng, "A Control Architecture for Quadruped Locomotion Over Rough Terrain", *International Conference on Robotics and Automation 2008*, pp. 811-818.

[25] M. Kalarkrishnan, J. Buchli, P. Pastor, S. Schaal, "Learning Locomotion over Rough Terrain using Terrain Templates", *International Conference on Intelligent Robots and Systems 2009*, pp. 167-172.